Chapter 2. Model Problems That Form Important Starting Points

The model problems discussed in this Chapter form the basis for chemists' understanding of the electronic states of atoms, molecules, nano-clusters, and solids as well as the rotational and vibrational motions and energy levels of molecules.

2.1 Free Electron Model of Polyenes

The particle-in-a-box type problems provide important models for several relevant chemical situations

The particle-in-a-box model for motion in one or two dimensions discussed earlier can obviously be extended to three dimensions. For two and three dimensions, it provides a crude but useful picture for electronic states on surfaces (i.e., when the electron can move freely on the surface but cannot escape to the vacuum or penetrate deeply into the solid) or in metallic crystals, respectively. I say metallic crystals because it is in such systems that the outermost valence electrons are reasonably well treated as moving freely rather than being tightly bound to a valence orbital on one of the constituent atoms or within chemical bonds localized to neighboring atoms.

Free motion within a spherical volume such as we discussed in Chapter 1 gives rise to eigenfunctions that are also used in nuclear physics to describe the motions of neutrons and protons in nuclei. In the so-called shell model of nuclei, the neutrons and protons fill separate s, p, d, etc. orbitals (refer back to Chapter 1 to recall how these orbitals are expressed in terms of spherical Bessel functions and what their energies are) with each type of nucleon forced to obey the Pauli principle (i.e., to have no more than two nucleons in each orbital because protons and neutrons are Fermions). For example, ^{4}He has two protons in 1s orbitals and 2 neutrons in 1s orbitals, whereas ^{3}He has two 1s protons and one 1s neutron. To remind you, I display in Fig. 2. 1 the angular shapes that characterize s, p, and d orbitals.
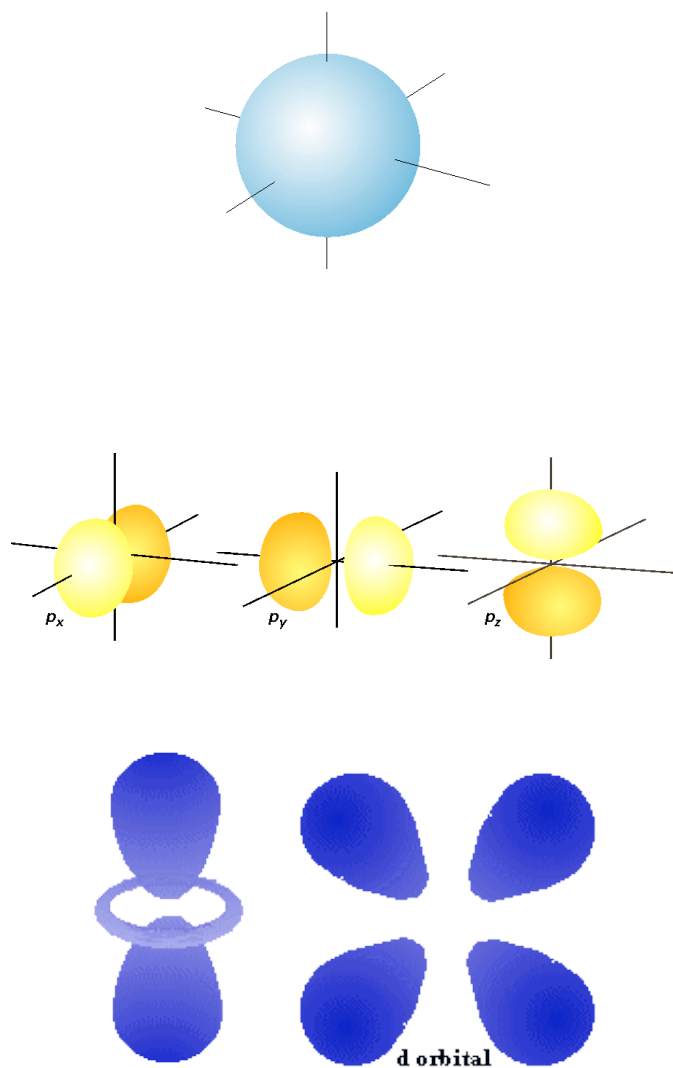
Figure 2.1. The angular shapes of s, p, and d functions

This same spherical box model has also been used to describe the valence electrons in quasi-spherical nano-clusters of metal atoms such as Cs_n, Cu_n, Na_n, Au_n, Ag_n, and their positive and negative ions. Because of the metallic nature of these species, their valence electrons are essentially free to roam over the entire spherical volume of the cluster, which renders this simple model rather effective. In this model, one thinks of each valence electron being free to roam within a sphere of radius R (i.e., having a potential that is uniform within the sphere and infinite outside the sphere).

The orbitals that solve the Schrödinger equation inside such a spherical box are not the same in their radial shapes as the s, p, d, etc. orbitals of atoms because, in atoms, there

is an additional attractive Coulomb radial potential $V(r) = -Ze^2/r$ present. In Chapter 1, we showed how the particle-in-a-sphere radial functions can be expressed in terms of spherical Bessel functions. In addition, the pattern of energy levels, which was shown in Chapter 1 to be related to the values of x at which the spherical Bessel functions $j_L(x)$ vanish, are not the same as in atoms, again because the radial potentials differ. However, the angular shapes of the spherical box problem are the same as in atomic structure because, in both cases, the potential is independent of θ and ϕ. As the orbital plots shown above indicate, the angular shapes of s, p, and d orbitals display varying number of nodal surfaces. The s orbitals have none, p orbitals have one, and d orbitals have two. Analogous to how the number of nodes related to the total energy of the particle constrained to the x, y plane, the number of nodes in the angular wave functions indicates the amount of angular or orbital rotational energy. Orbitals of s shape have no angular energy, those of p shape have less then do d orbitals, etc.

It turns out that the pattern of energy levels derived from this particle-in-a-spherical-box model can offer reasonably accurate descriptions of what is observed experimentally. In particular, when a cluster (or cluster ion) has a closed-shell electronic configuration in which, for a given radial quantum number n, all of the s, p, d orbitals associated with that n are doubly occupied, nanoscopic metal clusters are observed to display special stability (e.g., lack of chemical reactivity, large electron detachment energy). Clusters that produce such closed-shell electronic configurations are sometimes said to have magic-number sizes. The energy level expression given in Chapter 1

$$E_{L,n} = V_0 + (z_{L,n})^2\, \hbar^2/2mR^2$$

for an electron moving inside a sphere of radius R (and having a potential relative to the vacuum of V_0) can be used to model the energies of electron within metallic nano-clusters. Each electron occupies an orbital having quantum numbers n, L, and M, with the energies of the orbitals given above in terms of the zeros $\{z_{L,n}\}$ of the spherical Bessel functions. Spectral features of the nano-clusters are then determined by the energy gap between the highest occupied and lowest unoccupied orbital and can be tuned by

changing the radius (R) of the cluster or the charge (i.e., number of electrons) of the cluster.

Another very useful application of the model problems treated in Chapter 1 is the one-dimensional particle-in-a-box, which provides a qualitatively correct picture for π-electron motion along the p_π orbitals of delocalized polyenes. The one Cartesian dimension corresponds to motion along the delocalized chain. In such a model, the box length L is related to the carbon-carbon bond length R and the number N of carbon centers involved in the delocalized network L=(N-1) R. In Fig. 2.2, such a conjugated network involving nine centers is depicted. In this example, the box length would be eight times the C-C bond length.
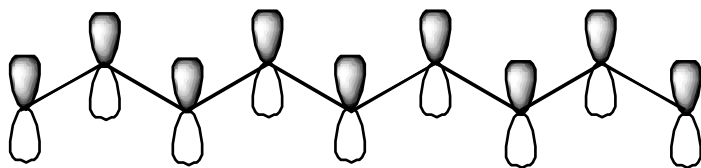
Conjugated π Network with 9 Centers Involved

Figure 2.2. The π atomic orbitals of a conjugated chain of nine carbon atoms, so the box length L is eight times the C-C bond length.

The eigenstates $\psi_n(x)$ and their energies E_n represent orbitals into which electrons are placed. In the example case, if nine π electrons are present (e.g., as in the 1,3,5,7-nonatetraene radical), the ground electronic state would be represented by a total wave function consisting of a product in which the lowest four ψ's are doubly occupied and the fifth ψ is singly occupied:

$$\Psi = \psi_1\alpha\psi_1\beta\psi_2\alpha\psi_2\beta\psi_3\alpha\psi_3\beta\psi_4\alpha\psi_4\beta\psi_5\alpha.$$

The z-component spin angular momentum states of the electrons are labeled α and β as discussed earlier.

We write the total wave function above as a product wave function because the total Hamiltonian involves the kinetic plus potential energies of nine electrons. To the extent that this total energy can be represented as the sum of nine separate energies, one for each electron, the Hamiltonian allows a separation of variables

$$H \cong \Sigma_{j=1,9} H(j)$$

in which each $H(j)$ describes the kinetic and potential energy of an individual electron. Of course, the full Hamiltonian contains electron-electron Coulomb interaction potentials $e^2/r_{i,j}$ that can not be written in this additive form. However, as we will treat in detail in Chapter 6, it is often possible to approximate these electron-electron interactions in a form that is additive.

Recall that when a partial differential equation has no operators that couple its different independent variables (i.e., when it is separable), one can use separation of variables methods to decompose its solutions into products. Thus, the (approximate) additivity of H implies that solutions of $H \psi = E \psi$ are products of solutions to

$$H (j) \psi(\mathbf{r}_j) = E_j \psi(\mathbf{r}_j).$$

The two lowest $\pi\pi*$ excited states would correspond to states of the form

$$\psi^* = \psi_1\alpha \, \psi_1\beta \, \psi_2\alpha \, \psi_2\beta \, \psi_3\alpha \, \psi_3\beta \, \psi_4\alpha \, \psi_5\beta \, \psi_5\alpha \text{ , and}$$

$$\psi'^* = \psi_1\alpha \, \psi_1\beta \, \psi_2\alpha \, \psi_2\beta \, \psi_3\alpha \, \psi_3\beta \, \psi_4\alpha \, \psi_4\beta \, \psi_6\alpha \text{ ,}$$

where the spin-orbitals (orbitals multiplied by α or β) appearing in the above products depend on the coordinates of the various electrons. For example,

$$\psi_1\alpha \ \psi_1\beta \ \psi_2\alpha \ \psi_2\beta \ \psi_3\alpha \ \psi_3\beta \ \psi_4\alpha \ \psi_5\beta \ \psi_5\alpha$$

denotes

$$\psi_1\alpha(\mathbf{r}_1) \ \psi_1\beta \ (\mathbf{r}_2) \ \psi_2\alpha \ (\mathbf{r}_3) \ \psi_2\beta \ (\mathbf{r}_4) \ \psi_3\alpha \ (\mathbf{r}_5) \ \psi_3\beta \ (\mathbf{r}_6) \ \psi_4\alpha \ (\mathbf{r}_7)\psi_5\beta \ (\mathbf{r}_8) \ \psi_5\alpha \ (\mathbf{r}_9).$$

The electronic excitation energies from the ground state to each of the above excited states within this model would be

$$\Delta E^* = \pi^2 \ \hbar^2/2m \ [\ 5^2/L^2 - 4^2/L^2] \text{ and}$$

$$\Delta E'^* = \pi^2 \ \hbar^2/2m \ [\ 6^2/L^2 - 5^2/L^2].$$

It turns out that this simple model of π-electron energies provides a qualitatively correct picture of such excitation energies. Its simplicity allows one, for example, to easily suggest how a molecule's color (as reflected in the complementary color of the light the molecule absorbs) varies as the conjugation length L of the molecule varies. That is, longer conjugated molecules have lower-energy orbitals because L^2 appears in the denominator of the energy expression. As a result, longer conjugated molecules absorb light of lower energy than do shorter molecules.

This simple particle-in-a-box model does not yield orbital energies that relate to ionization energies unless the potential inside the box is specified. Choosing the value of this potential V_0 that exists within the box such that $V_0 + \pi^2 \ \hbar^2/2m \ [\ 5^2/L^2]$ is equal to minus the lowest ionization energy of the 1,3,5,7-nonatetraene radical, gives energy levels (as $E = V_0 + \pi^2 \ \hbar^2/2m \ [\ n^2/L^2]$), which can then be used as approximations to ionization energies.

The individual π-molecular orbitals

$$\psi_n = (2/L)^{1/2} \sin(n\pi x/L)$$

are depicted in Fig. 2.3 for a model of the 1,3,5 hexatriene π-orbital system for which the box length L is five times the distance R_{CC} between neighboring pairs of carbon atoms. The magnitude of the kth C-atom centered atomic orbital in the nth π-molecular orbital is given by $(2/L)^{1/2} \sin(n\pi(k-1)R_{CC}/L)$.

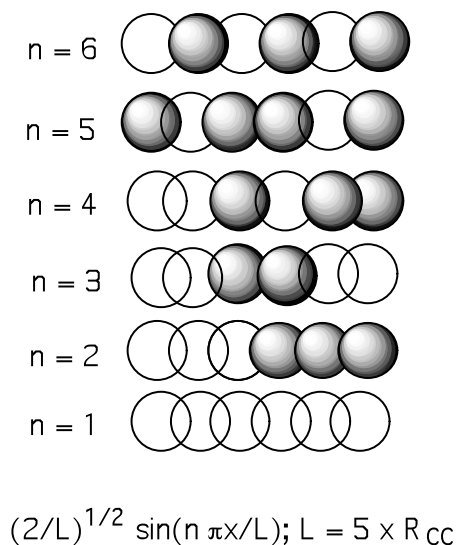$$(2/L)^{1/2} \sin(n \pi x/L); L = 5 \times R_{CC}$$

Figure 2.3. The phases of the six molecular orbitals of a chain containing six atoms.

In this figure, positive amplitude is denoted by the clear spheres, and negative amplitude is shown by the darkened spheres. Where two spheres of like shading overlap, the wave function has enhanced amplitude (i.e. there is a bonding interaction); where two spheres of different shading overlap, a node occurs (i.e., there is antibonding interaction). Once again, we note that the number of nodes increases as one ranges from the lowest-energy orbital to higher energy orbitals. The reader is once again encouraged to keep in mind this ubiquitous characteristic of quantum mechanical wave functions.

This simple model allows one to estimate spin densities at each carbon center and provides insight into which centers should be most amenable to electrophilic or nucleophilic attack. For example, radical attack at the C_5 carbon of the nine-atom

nonatetraene system described earlier would be more facile for the ground state ψ than for either ψ^* or ψ'^*. In the former, the unpaired spin density resides in ψ_5 (which varies as $\sin(5\pi x/8R_{CC})$ so is non-zero at $x = L/2$), which has non-zero amplitude at the C_5 site $x = L/2 = 4R_{CC}$. In ψ^* and ψ'^*, the unpaired density is in ψ_4 and ψ_6, respectively, both of which have zero density at C_5 (because $\sin(n\pi x/8R_{CC})$ vanishes for $n = 4$ or 6 at $x = 4R_{CC}$). Plots of the wave functions for n ranging from 1 to 7 are shown in another format in Fig. 2.4 where the nodal pattern is emphasized.
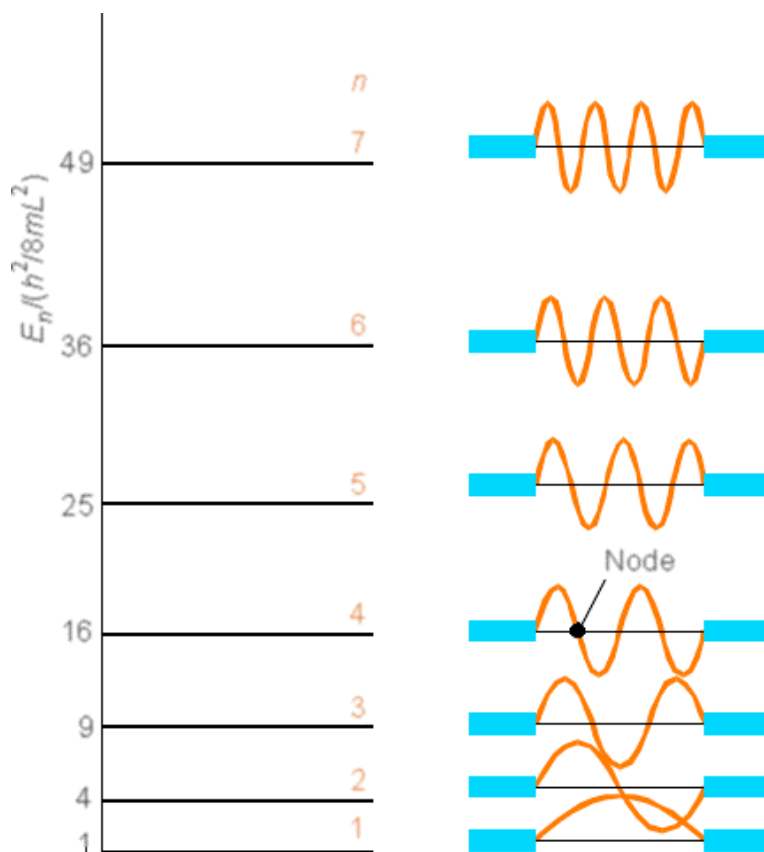

Figure 2.4. The nodal pattern for a chain containing seven atoms

I hope that by now the student is not tempted to ask how the electron gets from one region of high amplitude, through a node, to another high-amplitude region. Remember, such questions are cast in classical Newtonian language and are not appropriate when

addressing the wave-like properties of quantum mechanics.

2.2 Bands of Orbitals in Solids

Not only does the particle-in-a-box model offer a useful conceptual representation of electrons moving in polyenes, but it also is the zeroth-order model of band structures in solids. Let us consider a simple one-dimensional crystal consisting of a large number of atoms or molecules, each with a single orbital (the blue spheres shown below) that it contributes to the bonding. Let us arrange these building blocks in a regular lattice as shown in the Fig. 2.5.
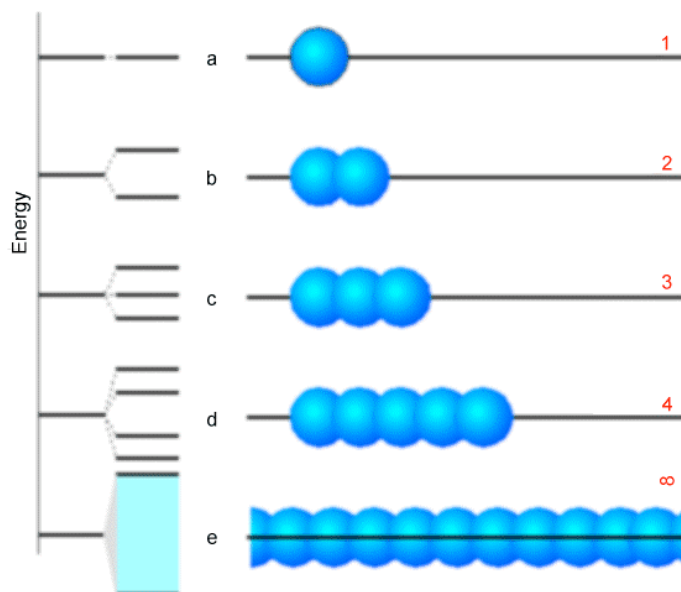
Figure 2.5. The energy levels arising from $1, 2, 3, 5$, and an infinite number of orbitals

In the top four rows of this figure we show the case with $1, 2, 3$, and 5 building blocks. To the left of each row, we display the energy splitting pattern into which the building blocks' orbitals evolve as they overlap and form delocalized molecular orbitals. Not surprisingly, for n = 2, one finds a bonding and an antibonding orbital. For n = 3, one has a bonding, one non-bonding, and one antibonding orbital. Finally, in the bottom row, we attempt to show what happens for an infinitely long chain. The key point is that the discrete number of molecular orbitals appearing in the 1-5 orbital cases evolves into a continuum of orbitals called a band as the number of building blocks becomes large. This

band of orbital energies ranges from its bottom (whose orbital consists of a fully in-phase bonding combination of the building block orbitals) to its top (whose orbital is a fully out-of-phase antibonding combination).

In Fig. 2.6 we illustrate these fully bonding and fully antibonding band orbitals for two cases- the bottom involving s-type building block orbitals, and the top involving p_σ-type orbitals. Notice that when the energy gap between the building block s and p_σ orbitals is larger than is the dispersion (spread) in energy within the band of s or band of p_σ orbitals, a band gap occurs between the highest member of the s band and the lowest member of the p_σ band. The splitting between the s and p_σ orbitals is a property of the individual atoms comprising the solid and varies among the elements of the periodic table. For example, we teach students that the 2s-2p energy gap in C is smaller than the 3s-3p gap in Si, which is smaller than the 4s-4p gap in Ge. The dispersion in energies that a given band of orbitals is split into as these atomic orbitals combine to form a band is determined by how strongly the orbitals on neighboring atoms overlap. Small overlap produces small dispersion, and large overlap yields a broad band. So, the band structure of any particular system can vary from one in which narrow bands (weak overlap) do not span the energy gap between the energies of their constituent atomic orbitals to bands that overlap strongly (large overlap).
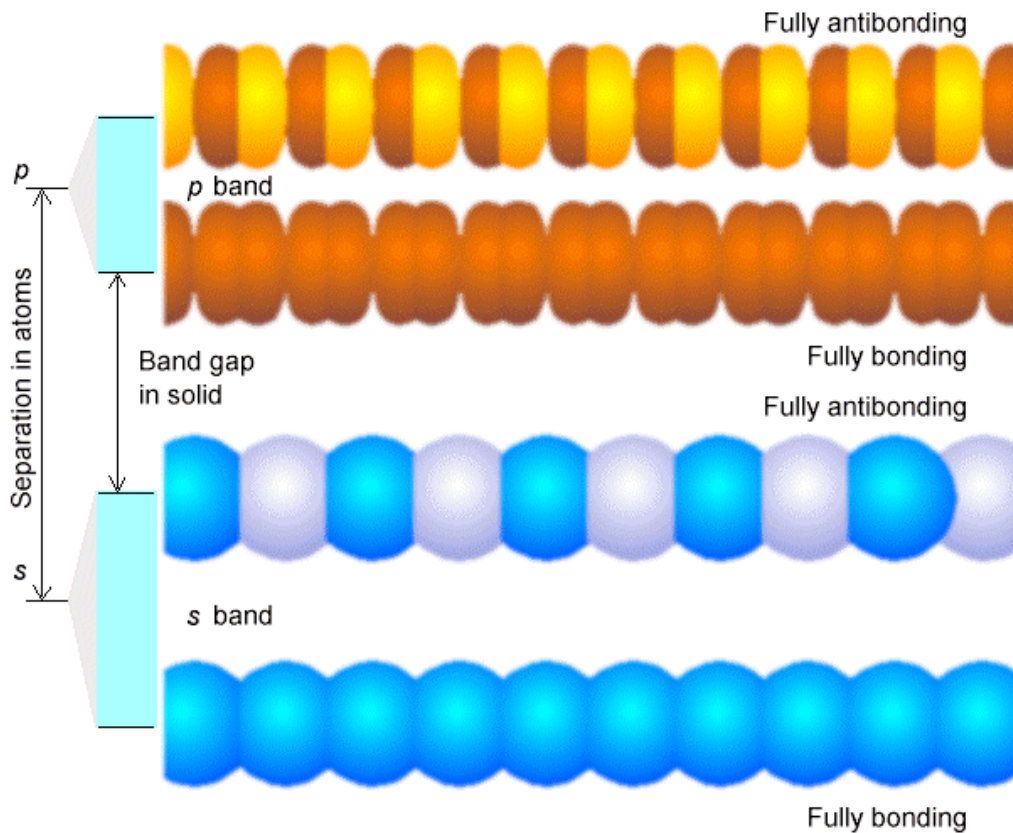
Figure 2.6. The bonding through antibonding energies and band orbitals arising from s and from p_σ atomic orbitals.

Depending on how many valence electrons each building block contributes, the various bands formed by overlapping the building-block orbitals of the constituent atoms will be filled to various levels. For example, if each building block orbital shown above has a single valence electron in an s-orbital (e.g., as in the case of the alkali metals), the s-band will be half filled in the ground state with α and β -paired electrons. Such systems produce very good conductors because their partially filled s bands allow electrons to move with very little (e.g., only thermal) excitation among other orbitals in this same band. On the other hand, for alkaline earth systems with two s electrons per atom, the s-band will be completely filled. In such cases, conduction requires excitation to the lowest members of the nearby p-orbital band. Finally, if each building block were an Al ($3s^2\ 3p^1$)

atom, the s-band would be full and the p-band would be half filled. In Fig. 2.6 a, we show a qualitative depiction of the bands arising from sodium atoms' 1s, 2s, 2p, and 3s orbitals. Notice that the 1s band is very narrow because there is little coupling between neighboring 1s orbitals, so they are only slightly stabilized or destabilized relative to their energies in the isolated Na atoms. In contrast, the 2s and 2p bands show greater dispersion (i.e., are wider), and the 3s band is even wider. The 1s, 2s, and 2p bands are full, but the 3s band is half filled, as a result of which solid Na is a good electrical conductor.
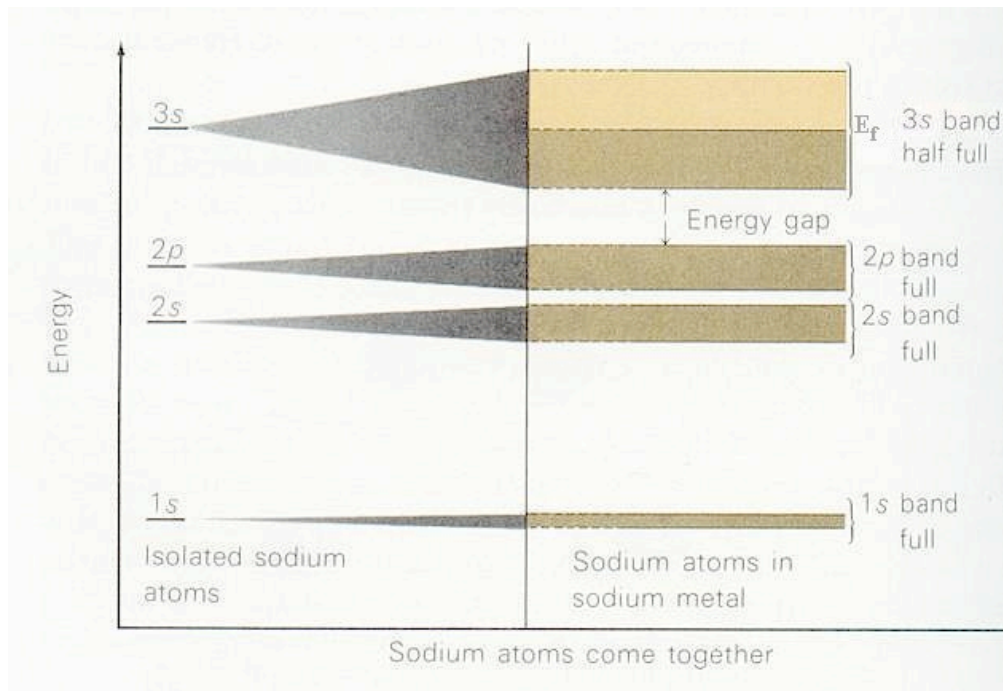

Figure 2.6 a. Example of sodium atoms' 1s, 2s, 2p, and 3s orbitals splitting into filled and partially filled bands in sodium metal.

In describing the band of states that arise from a given atomic orbital within a solid, it is common to display the variation in energies of these states as functions of the number of sign changes in the coefficients that describe each orbital as a linear combination of the constituent atomic orbitals. Using the one-dimensional array of s and p_σ orbitals shown in Fig. 2.6 as an example,

(1) the lowest member of the band deriving from the s orbitals

$$\phi_0 = s(1) + s(2) + s(3) + s(4) + ... + s(N)$$

is a totally bonding combination of all of the constituent s orbitals on the N sites of the lattice.

(2) The highest-energy orbital in this band

$$\phi_N = s(1) - s(2) + s(3) - s(4) + ... + s(N-1) - s(N)$$

is a totally anti-bonding combination of the constituent s orbitals.

(3) Each of the intervening orbitals in this band has expansion coefficients that allow the orbital to be written as

$$\phi_n = \sum_{j=1}^{N} \cos(\frac{n(j-1)\pi}{N}) s(j)$$

Clearly, for small values of n, the series of expansion coefficients $\cos(\frac{n(j-1)\pi}{N})$ has few sign changes as the index j runs over the sites of the one-dimensional lattice. For larger n, there are more sign changes. Thus, thinking of the quantum number n as labeling the number of sign changes and plotting the energies of the orbitals (on the vertical axis) versus n (on the horizontal axis), we would obtain a plot that increases from n = 0 to n =N. In fact, such plots tend to display quadratic variation of the energy with n. This observation can be understood by drawing an analogy between the pattern of sign changes belonging to a particular value of n and the number of nodes in the one-dimensional particle-in-a-box wave function, which also is used to model electronic states delocalized along a linear chain. As we saw in Chapter 1, the energies for this model system varied as

$$E = \frac{j^2 \pi^2 \hbar^2}{2mL^2}$$

with j being the quantum number ranging from 1 to ∞. The lowest-energy state, with j = 1, has no nodes; the state with j = 2 has one node, and that with j = n has (n-1) nodes. So, if we replace j by (n-1) and replace the box length L by (NR), where R is the inter-atom spacing and N is the number of atoms in the chain, we obtain

$$E = \frac{(n-1)^2 \pi^2 \hbar^2}{2mN^2 R^2}$$

from which on can see why the energy can be expected to vary as $(n/N)^2$.

(4) In contrast for the p_σ orbitals, the lowest-energy orbital is

$$\phi_0 = p_\sigma(1) - p_\sigma(2) + p_\sigma(3) - p_\sigma(4) + \ldots - p_\sigma(N-1) + p_\sigma(N)$$

because this alternation in signs allows each p_σ orbital on one site to overlap in a bonding fashion with the p_σ orbitals on neighboring sites.

(5) Therefore, the highest-energy orbital in the p_σ band is

$$\phi_N = p_\sigma(1) + p_\sigma(2) + p_\sigma(3) + p_\sigma(4) + \ldots + p_\sigma(N-1) + p_\sigma(N)$$

and is totally anti-bonding.

(6) The intervening members of this band have orbitals given by

$$\phi_{N-n} = \sum_{j=1}^{N} \cos(\frac{n(j-1)\pi}{N}) s(j)$$

with low n corresponding to high-energy orbitals (having few inter-atom sign changes but anti-bonding character) and high n to low-energy orbitals (having many inter-atom sign changes). So, in contrast to the case for the s-band orbitals, plotting the energies of the

orbitals (on the vertical axis) versus n (on the horizontal axis), we would obtain a plot that decreases from n = 0 to n =N.

For bands comprised of p_π orbitals, the energies vary with the n quantum number in a manner analogous to how the s band varies because the orbital with no inter-atom sign changes is fully bonding. For two- and three-dimensional lattices comprised of s, p, and d orbitals on the constituent atoms, the behavior of the bands derived from these orbitals follows analogous trends. It is common to describe the sign alternations arising from site to site in terms of a so-called **k** vector. In the one-dimensional case discussed above, this vector has only one component with elements labeled by the ratio (n/N) whose value characterizes the number of inter-atom sign changes. For lattices containing many atoms, N is very large, so n ranges from zero to a very large number. Thus, the ratio (n/N) ranges from zero to unity in small fractional steps, so it is common to think of these ratios as describing a continuous parameter varying from zero to one. Moreover, it is convention to allow the n index to range from –N to +N, so the argument n π /N in the cosine function introduced above varies from – π to +π.

In two- or three-dimensions the **k** vector has two or three elements and can be written in terms of its two or three index ratios, respectively, as

$$k_2 = (\frac{n}{N}, \frac{m}{M})$$

$$k_3 = (\frac{n}{N}, \frac{m}{M}, \frac{l}{L}).$$

Here, N, M, and L would describe the number of unit cells along the three principal axes of the three-dimensional crystal; N and M do likewise in the two-dimensional lattice case.

In such two- and three- dimensional crystal cases, the energies of orbitals within bands derived from s, p, d, etc. atomic orbitals display variations that also reflect the number of inter-atom sign changes. However, now there are variations as functions of the (n/N), (n/M) and (l/L) indices, and these variations can display rather complicated shapes depending on the symmetry of the atoms within the underlying crystal lattice. That is, as

one moves within the three-dimensional space by specifying values of the indices (n/N), (n/M) and (l/L), one can move throughout the lattice in different symmetry directions. It is convention in the solid-state literature to plot the energies of these bands as these three indices vary from site to site along various symmetry elements of the crystal and to assign a letter to label this symmetry element. The band that has no inter-atom sign changes is labeled as Γ (sometimes G) in such plots of band structures. In much of our discussion below, we will analyze the behavior of various bands in the neighborhood of the Γ point because this is where there are the fewest inter-atom nodes and thus the wave function is easiest to visualize.

Let's consider a few examples to help clarify these issues. In Fig. 2.6 b, where we see the band structure of graphene, you can see the quadratic variations of the energies with k as one moves away from the k = 0 point labeled Γ, with some bands increasing with k and others decreasing with k.
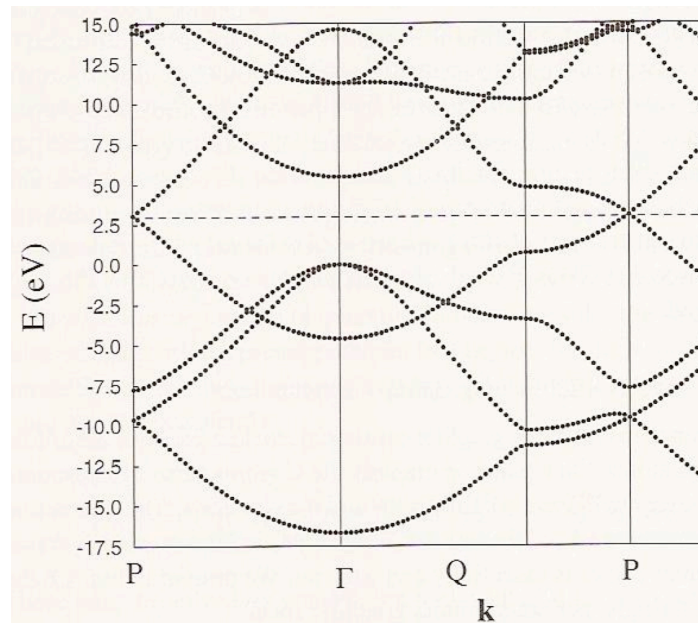

Figure 2.6 b Band structure plot for graphene.

The band having an energy of ca. -17 eV at the Γ point originates from bonding interactions involving 2s orbitals on the carbon atoms, while those having energies near 0 eV at the Γ point derive from carbon $2p_\sigma$ bonding interactions. The parabolic increase

with k for the 2s-based and decrease with k for the $2p_\sigma$-based orbitals is clear and is expected based on our earlier discussion of how s and p_σ bands vary with k. The band having energy near -4 eV at the Γ point involves $2p_\pi$ orbitals involved in bonding interactions, and this band shows a parabolic increase with k as expected as we move away from the Γ point. These are the delocalized π orbitals of the graphene sheet. The anti-bonding $2p_\pi$ band decreases quadratically with k and has an energy of ca. 15 eV at the Γ point. Because there are two atoms per unit cell in this case, there are a total of eight valence electrons (four from each carbon atom) to be accommodated in these bands. The eight carbon valence electrons fill the bonding 2s and two $2p_\sigma$ bands fully as well as the bonding $2p_\pi$ band. Only along the direction labeled P in Fig. 2.6 b do the bonding and anti-bonding $2p_\pi$ bands become degenerate (near 2.5 eV); the approach of these two bands is what allows graphene to be semi-metallic (i.e., to conduct at modest temperatures- high enough to promote excitations from the bonding $2p_\pi$ to the anti-bonding $2p_\pi$ band).

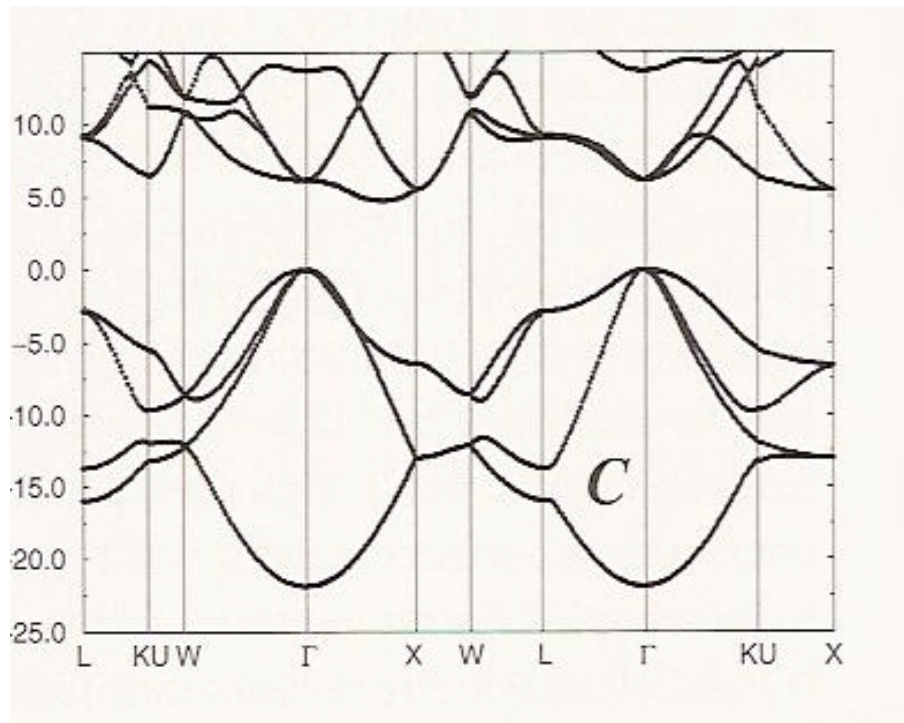It is interesting to contrast the band structure of graphene with that of diamond, which is shown in Fig. 2. 6 c.

Figure 2.6 c Band structure of diamond carbon.

The band having an energy of ca. – 22 eV at the Γ point derives from 2s bonding interactions, and the three bands near 0 eV at the Γ point come from $2p_\sigma$ bonding interactions. Again, each of these bands displays the expected parabolic behavior as functions of k. In diamond's two interpenetrating face centered cubic structure, there are two carbon atoms per unit cell, so we have a total of eight valence electrons to fill the four bonding bands. Notice that along no direction in k-space do these filled bonding bands become degenerate with or are crossed by any of the other bands. The other bands remain at higher energy along all k-directions, and thus there is a gap between the bonding bands and the others is large (ca. 5 eV or more along any direction in k-space). This is why diamond is an insulator; the band gap is very large.

Finally, let's compare the graphene and diamond cases with a metallic case such as shown in Fig. 2. 6 d for Al and for Ag.
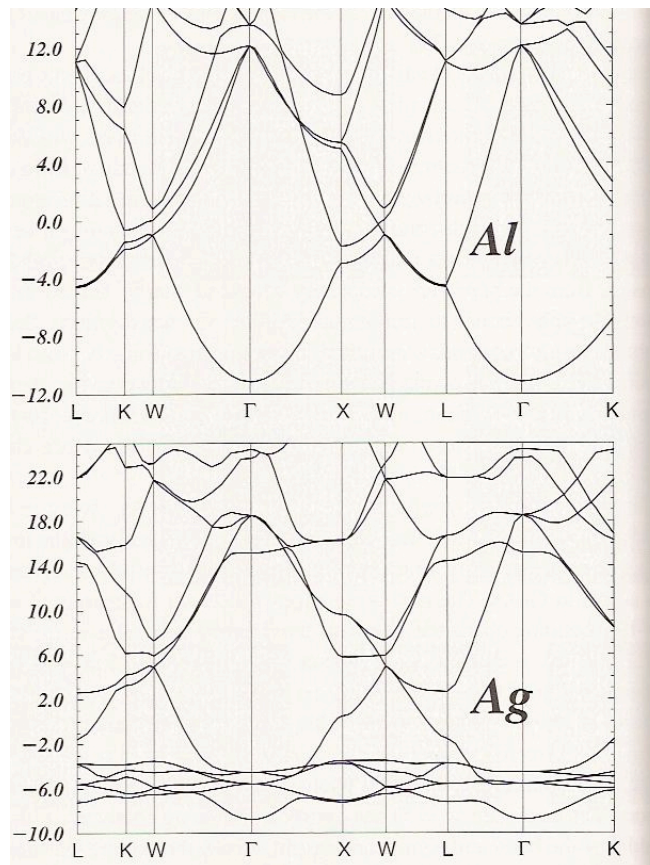

Figure 2. 6 d Band structures of Al and Ag.

For Al and Ag, there is one atom per unit cell, so we have three valence electrons ($3s^2 3p^1$) and eleven valence electrons ($3d^{10} 4s^1$), respectively, to fill the bands shown in Fig. 2. 6 d. Focusing on the Γ points in the Al and Ag band structure plots, we can say the following:

1. For Al, the 3s-based band near -11 eV is filled and the three 3p-based bands near 11 eV have an occupancy of 1/6 (i.e., on average there is one electron in one of these three bands each of which can hold two electrons).

2. The 3s and 3p bands are parabolic with positive and negative curvature, respectively.

3. Along several directions (e.g. K, W, X, W, L) there are crossings among the bands; these crossings allow electrons to be promoted from occupied to previously unoccupied bands. The partial occupancy of the 3p bands and the multiple crossings of bands are what allow Al to show metallic behavior.

4. For Ag, there are six bands between -4 eV and -8 eV. Five of these bands change little with k, and one shows somewhat parabolic dependence on k. The former five derive from 4d atomic orbitals that are contracted enough to not allow them to overlap much, and the latter is based on 5s bonding orbital interaction.

5. Ten of the valence electrons fill the five 4d bands, and the eleventh resides in the 5s-based bonding band.

6. If the five 4d-based bands are ignored, the remainder of the Ag band structure looks a lot like that for Al. There are numerous band crossings that include, in particular, the half-filled 5s band. These crossings and the partial occupancy of the 5s band cause Ag to have metallic character.

One more feature of band structures that is often displayed is called the band density of states. An example of such a plot is shown in Fig. 2. 6 e for the TiN crystal.
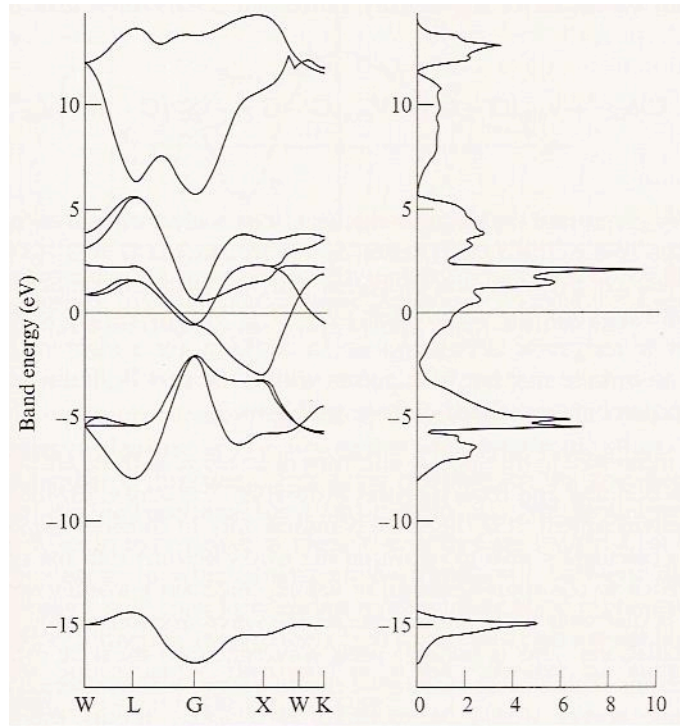
Figure 2.6 e. Energies of orbital bands in TiN along various directions in **k**-space (left) and densities of states (right) as functions of energy for this same crystal.

The density of states at energy E is computed by summing all those orbitals having an energy between E and E + dE. Clearly, as seen in Fig. 2.6 e, for bands in which the orbital energies vary strongly with **k** (i.e., so-called broad bands), the density of states is low; in contrast, for narrow bands, the density of states is high. The densities of states are important because their energies and energy spreads relate to electronic spectral features. Moreover, just as gaps between the highest occupied bands and the lowest unoccupied bands play central roles in determining whether the sample is an insulator, a conductor, or a semiconductor, gaps in the density of states suggest what frequencies of light will be absorbed or reflected via inter-band electronic transitions.

The bands of orbitals arising in any solid lattice provide the orbitals that are available to be occupied by the number of electrons in the crystal. Systems whose highest energy occupied band is completely filled and for which the gap in energy to the lowest unfilled band is large are called insulators because they have no way to easily (i.e., with little energy requirement) promote some of their higher-energy electrons from orbital to orbital and thus effect conduction. The case of diamond discussed above is an example of

an insulator. If the band gap between a filled band and an unfilled band is small, it may be possible for thermal excitation (i.e., collisions with neighboring atoms or molecules) to cause excitation of electrons from the former to the latter thereby inducing conductive behavior. The band structures of Al and Ag discussed above offer examples of this case. A simple depiction of how thermal excitations can induce conduction is illustrated in Fig. 2.7.

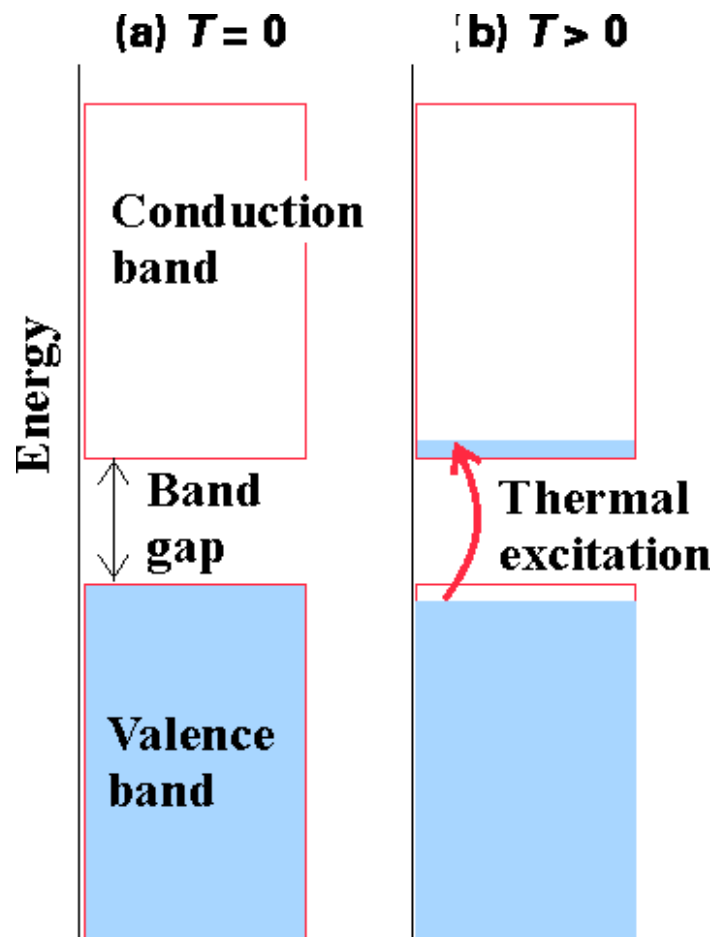Figure 2.7. The valence and conduction bands and the band gap with a small enough gap to allow thermal excitation to excite electrons and create holes in a previously filled band.

Systems whose highest-energy occupied band is partially filled are also conductors because they have little spacing among their occupied and unoccupied orbitals so electrons can flow easily from one to another. Al and Ag are good examples.

To form a semiconductor, one starts with an insulator whose lower band is filled and whose upper band is empty as shown by the broad bands in Fig.2.8.
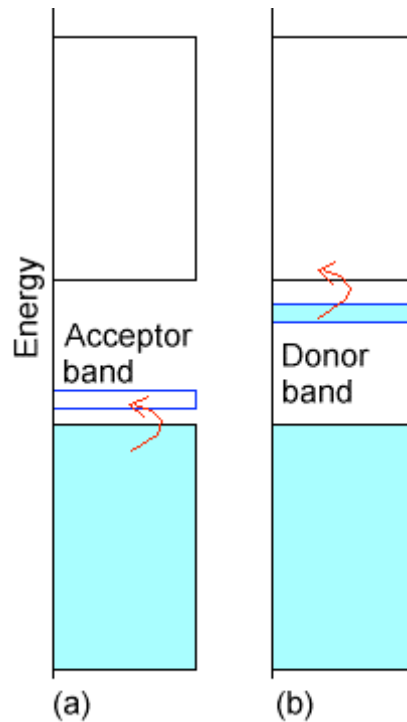

Figure 2.8. The filled and empty bands, the band gap, and empty acceptor or filled donor bands.

If this insulator material is synthesized with a small amount of "dopant" whose valence orbitals have energies between the filled and empty bands of the insulator, one can generate a semiconductor. If the dopant species has no valence electrons (i.e., has an empty valence orbital), it gives rise to an empty band lying between the filled and empty bands of the insulator as shown below in case a of Fig. 2.8. In this case, the dopant band can act as an electron acceptor for electrons excited (either thermally or by light) from the filled band of the insulator into the dopant's empty band. Once electrons enter the dopant band, charge can flow (because the insulator's lower band is no longer filled) and the system thus becomes a conductor. Another case is illustrated in the b part of Fig. 2.8. Here, the dopant has a filled band that lies close in energy to the empty band of the insulator. Excitation of electrons from this dopant band to the insulator's empty band can

116

induce current to flow (because now the insulator's upper band is no longer empty).

2.3 Densities of States in 1, 2, and 3 dimensions.

When a large number of neighboring orbitals overlap, bands are formed. However, the natures of these bands, their energy patterns, and their densities of states are very different in different dimensions.

Before leaving our discussion of bands of orbitals and orbital energies in solids, I want to address a bit more the issue of the density of electronic states and what determines the energy range into which orbitals of a given band will split. First, let's recall the energy expression for the 1 and 2- dimensional electron in a box case, and let's generalize it to three dimensions. The general result is

$$E = \Sigma_j \, n_j^2 \, \pi^2 \, \hbar^2/(2mL_j^2)$$

where the sum over j runs over the number of dimensions (1, 2, or 3), and L_j is the length of the box along the jth direction. For one dimension, one observes a pattern of energy levels that grows with increasing n, and whose spacing between neighboring energy levels also grows as a result of which the state density decreases with increasing n. However, in 2 and 3 dimensions, the pattern of energy level spacing displays a qualitatively different character, especially at high quantum number.

Consider first the 3-dimensional case and, for simplicity, let's use a box that has equal length sides L. In this case, the total energy E is $(\hbar^2\pi^2/2mL^2)$ times $(n_x^2 + n_y^2 + n_z^2)$. The latter quantity can be thought of as the square of the length of a vector R having three components n_x, n_y, n_z. Now think of three Cartesian axes labeled n_x, n_y, and n_z and view a sphere of radius R in this space. The volume of the $1/8^{th}$ sphere having positive values of n_x, n_y, and n_z and having radius R is 1/8 $(4/3 \, \pi R^3)$. Because each cube having unit length along the n_x, n_y, and n_z axes corresponds to a single quantum wave function and its energy, the total number $N_{tot}(E)$ of quantum states with positive n_x, n_y, and n_z and with energy between zero and $E = (\hbar^2\pi^2/2mL^2)R^2$ is

$$N_{tot} = 1/8 \ (4/3 \ \pi R^3) = 1/8 \ (4/3 \ \pi \ [2mEL^2/(\hbar^2\pi^2)])^{3/2}$$

The number of quantum states with energies between E and E+dE is (dN_{tot}/dE) dE, which gives the density $\Omega(E)$ of states near energy E:

$$\Omega(E) = (dN_{tot}/dE) = 1/8 \ (4/3 \ \pi \ [2mL^2/(\hbar^2\pi^2)])^{3/2} \ 3/2 \ E^{1/2}.$$

Notice that this state density increases as E increases. This means that, in the 3-dimensional case, the number of quantum states per unit energy grows; in other words, the spacing between neighboring state energies decreases, very unlike the 1-dimensioal case where the spacing between neighboring states grows as n and thus E grows. This growth in state density in the 3-dimensional case is a result of the degeneracies and near-degeneracies that occur. For example, the states with n_x, n_y, $n_z = 2,1,1$ and 1, 1, 2, and 1, 2, 1 are degenerate, and those with n_x, n_y, $n_z = 5, 3, 1$ or 5, 1, 3 or 1, 3, 5 or 1, 5, 3 or 3, 1, 5 or 3, 5, 1 are degenerate and nearly degenerate to those having quantum numbers 4, 4, 1 or 1, 4, 4, or 4, 1, 4.

In the 2-dimensional case, degeneracies also occur and cause the density of states to possess an E-dependence that differs from the 1- or 3-dimensional case. In this situation
, we think of states having energy E = $(\hbar^2\pi^2/2mL^2)R^2$, but with $R^2 = n_x^2 + n_y^2$. The total number of states having energy between zero and E is

$$N_{total} = 4\pi R^2 = 4\pi \ E(2mL^2/\hbar^2\pi^2)$$

So, the density of states between E and E+dE is

$$\Omega(E) = dN_{total}/dE = 4\pi \ (2mL^2/\hbar^2\pi^2)$$

That is, in this 2-dimensional case, the number of states per unit energy is constant for high E values (where the analysis above applies best).

This kind of analysis for the 1-dimensional case gives

$$N_{total} = R = (2mEL^2/\hbar^2\pi^2)^{1/2}$$

so, the state density between E and E+ dE is:

$$\Omega(E) = 1/2 \ (2mL^2/\hbar^2\pi^2)^{1/2} \ E^{-1/2},$$

which clearly shows the widening spacing, and thus lower state density, as one goes to higher energies.

These findings about densities of states in 1-, 2-, and 3- dimensions are important because, in various problems one encounters in studying electronic states of extended systems such as solids, chains, and surfaces, one needs to know how the number of states available at a given total energy E varies with E. A similar situation occurs when describing the translational states of an electron or a photo ejected from an atom or molecule into the vacuum; here the 3-dimensional density of states applies. Clearly, the state density depends upon the dimensionality of the problem, and this fact is what I want the students reading this text to keep in mind.

Before closing this Section, it is useful to overview how the various particle-in-box models can be used as qualitative descriptions for various chemical systems.

1a. The one-dimensional box model is most commonly used to model electronic orbitals in delocalized linear polyenes.

1b. The electron-on-a-circle model is used to describe orbitals in a conjugated cyclic ring such as in benzene.

2a. The rectangular box model can be used to model electrons moving within thin layers of metal deposited on a substrate or to model electrons in aromatic sheets such as graphene shown below in Fig. 2.8a.
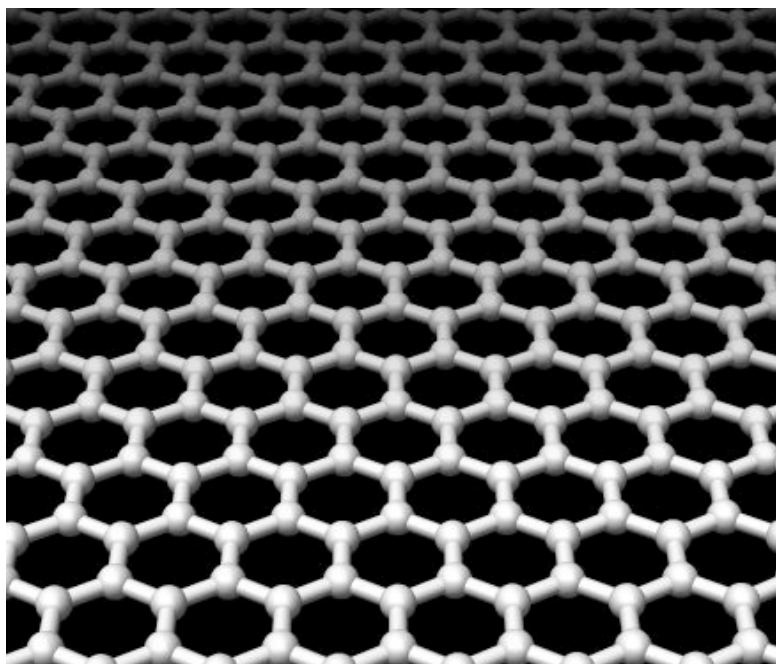
Figure 2.8a Depiction of the aromatic rings of graphene extending in two dimensions.

2b. The particle-within-a-circle model can describe states of electrons (or other light particles requiring quantum treatment) constrained within a circular corral.

2c. The particle-on-a-sphere's surface model can describe states of electrons delocalized over the surface of fullerene-type species such as shown in the upper right of Fig. 2.8b.

Figure 2.8b Fullerene (upper right) and tubes of rolled up graphenes (lower three).

3a. The particle-in-a-sphere model, as discussed earlier, is often used to treat electronic orbitals of quasi-spherical nano-clusters composed of metallic atoms.

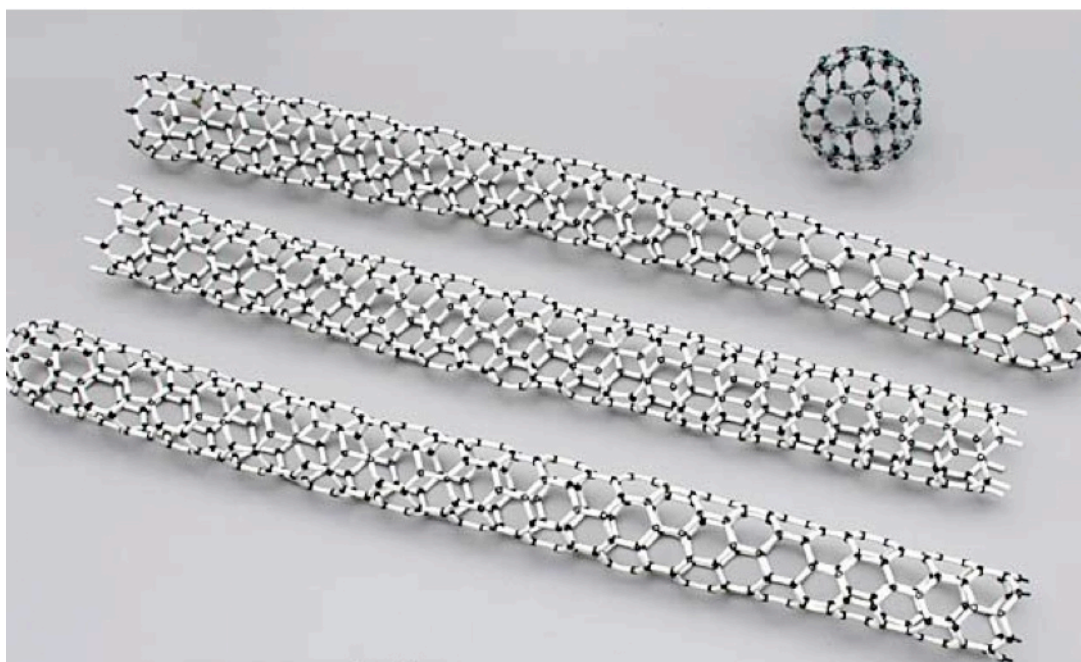3b. The particle-in-a-cube model is often used to describe the bands of electronic orbitals that arise in three-dimensional crystals constructed from metallic atoms.

In all of these models, the potential V_0, which is constant in the region where the electron is confined, controls the energies of all the quantum states relative to that of a free electron (i.e., an electron in vacuum with no kinetic energy).

For some dimensionalities and geometries, it may be necessary to invoke more than one of these models to qualitatively describe the quantum states of systems for which the valence electrons are highly delocalized (e.g., metallic clusters and conjugated organics). For example, for electrons residing on the surface of any of the three graphene tubes shown in Fig. 2.8b, one expects quantum states (i) labeled with an angular momentum quantum number and characterizing the electrons' angular motions about the long axis of the tube, but also (ii) labeled by a long-axis quantum number characterizing the electron's energy component along the tube's long axis. For a three-dimensional tube-shaped nanoparticle composed of metallic atoms, one expects the quantum states to be (i) labeled with an angular momentum quantum number and a radial quantum number characterizing the electrons' angular motions about the long axis of the tube and its radial (Bessel function) character, but again also (ii) labeled by a long-axis quantum number characterizing the electron's energy component along the tube's long axis.

2.4 The Most Elementary Model of Orbital Energy Splittings: Hückel or Tight Binding Theory

Now, let's examine what determines the energy range into which orbitals (e.g., p_π orbitals in polyenes, metal, semi-conductor, or insulator; s or p_σ orbitals in a solid; or σ or π atomic orbitals in a molecule) split. I know that, in our earlier discussion, we talked about the degree of overlap between orbitals on neighboring atoms relating to the energy splitting, but now it is time to make this concept more quantitative. To begin, consider two orbitals, one on an atom labeled A and another on a neighboring atom labeled B;

these orbitals could be, for example, the 1s orbitals of two hydrogen atoms, such as Figure 2.9 illustrates.
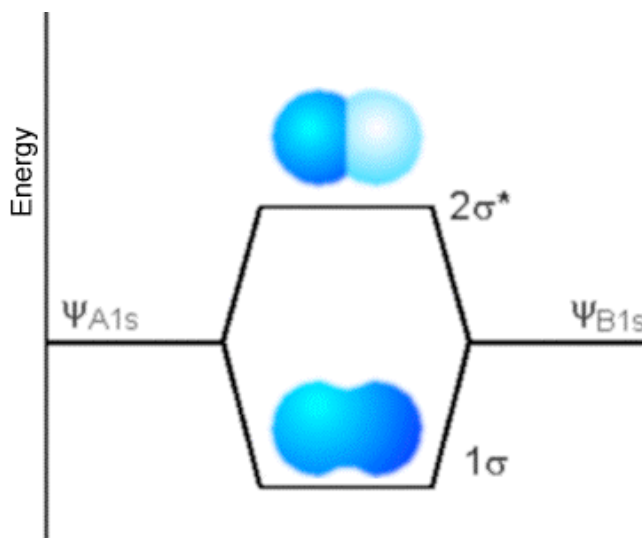

Figure 2.9. Two 1s orbitals combine to produce a σ bonding and a σ* antibonding molecular orbital

However, the two orbitals could instead be two p_π orbitals on neighboring carbon atoms such as are shown in Fig. 2.10 as they form π bonding and π* anti-bonding orbitals.
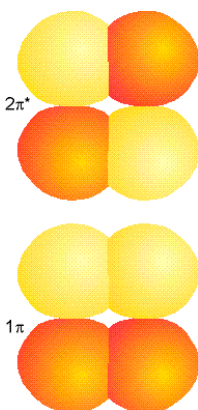

Figure 2.10. Two atomic p_π orbitals form a bonding π and antibonding π* molecular orbital.

In both of these cases, we think of forming the molecular orbitals (MOs) ϕ_k as linear combinations of the atomic orbitals (AOs) χ_a on the constituent atoms, and we express this mathematically as follows:

$$\phi_K = \Sigma_a C_{K,a} \chi_a,$$

where the $C_{K,a}$ are called linear combination of atomic orbital to form molecular orbital (LCAO-MO) coefficients. The MOs are supposed to be solutions to the Schrödinger equation in which the Hamiltonian H involves the kinetic energy of the electron as well as the potentials V_L and V_R detailing its attraction to the left and right atomic centers (this one-electron Hamiltonian is only an approximation for describing molecular orbitals; more rigorous N-electron treatments will be discussed in Chapter 6):

$$H = - \hbar^2/2m \, \nabla^2 + V_L + V_R.$$

In contrast, the AOs centered on the left atom A are supposed to be solutions of the Schrödinger equation whose Hamiltonian is $H = - \hbar^2/2m \, \nabla^2 + V_L$, and the AOs on the right atom B have $H = - \hbar^2/2m \, \nabla^2 + V_R$. Substituting $\phi_K = \Sigma_a C_{K,a} \chi_a$ into the MO's Schrödinger equation

$$H\phi_K = \varepsilon_K \, \phi_K$$

and then multiplying on the left by the complex conjugate of χ_b and integrating over the r, θ and ϕ coordinates of the electron produces

$$\Sigma_a <\chi_b| - \hbar^2/2m \, \nabla^2 + V_L + V_R |\chi_a> C_{K,a} = \varepsilon_K \Sigma_a <\chi_b|\chi_a> C_{K,a}$$

Recall that the Dirac notation <a|b> denotes the integral of a* and b, and <a| op| b> denotes the integral of a* and the operator op acting on b.

In what is known as the Hückel model in chemistry or the tight-binding model in

solid-state theory, one approximates the integrals entering into the above set of linear equations as follows:

i. The diagonal integral $\langle\chi_b| - \hbar^2/2m\, \nabla^2 + V_L + V_R |\chi_b\rangle$ involving the AO centered on the right atom and labeled χ_b is assumed to be equivalent to $\langle\chi_b| - \hbar^2/2m\, \nabla^2 + V_R |\chi_b\rangle$, which means that net attraction of this orbital to the left atomic center is neglected. Moreover, this integral is approximated in terms of the binding energy (denoted α, not to be confused with the electron spin function α) for an electron that occupies the χ_b orbital: $\langle\chi_b| - \hbar^2/2m\, \nabla^2 + V_R |\chi_b\rangle = \alpha_b$. The physical meaning of α_b is the kinetic energy of the electron in χ_b plus the attraction of this electron to the right atomic center while it resides in χ_b. Of course, an analogous approximation is made for the diagonal integral involving χ_a; $\langle\chi_a| - \hbar^2/2m\, \nabla^2 + V_L |\chi_a\rangle = \alpha_a$. These α values are negative quantities because, as is convention in electronic structure theory, energies are measured relative to the energy of the electron when it is removed from the orbital and possesses zero kinetic energy.

ii. The off-diagonal integrals $\langle\chi_b| - \hbar^2/2m\, \nabla^2 + V_L + V_R |\chi_a\rangle$ are expressed in terms of a parameter $\beta_{a,b}$ which relates to the kinetic and potential energy of the electron while it resides in the "overlap region" in which both χ_a and χ_b are non-vanishing. This region is shown pictorially above as the region where the left and right orbitals touch or overlap. The magnitude of β is assumed to be proportional to the overlap $S_{a,b}$ between the two AOs : $S_{a,b} = \langle\chi_a|\chi_b\rangle$. It turns out that β is usually a negative quantity, which can be seen by writing it as $\langle\chi_b| - \hbar^2/2m\, \nabla^2 + V_R |\chi_a\rangle + \langle\chi_b| V_L |\chi_a\rangle$. Since χ_a is an eigenfunction of $-\hbar^2/2m\, \nabla^2 + V_R$ having the eigenvalue α_a, the first term is equal to α_a (a negative quantity) times $\langle\chi_b|\chi_a\rangle$, the overlap S. The second quantity $\langle\chi_b| V_L |\chi_a\rangle$ is equal to the integral of the overlap density $\chi_b(r)\,\chi_a(r)$ multiplied by the (negative) Coulomb potential for attractive interaction of the electron with the left atomic center. So, whenever $\chi_b(r)$ and $\chi_a(r)$ have positive overlap, β will turn out negative.

iii. Finally, in the most elementary Hückel or tight-binding model, the off-diagonal overlap integrals $\langle\chi_a|\chi_b\rangle = S_{a,b}$ are neglected and set equal to zero on the right side of the matrix eigenvalue equation. However, in some Hückel models, overlap between neighboring orbitals is explicitly treated, so, in some of the discussion below we will retain $S_{a,b}$.

With these Hückel approximations, the set of equations that determine the orbital energies ε_K and the corresponding LCAO-MO coefficients $C_{K,a}$ are written for the two-orbital case at hand as in the first 2x2 matrix equations shown below

$$\begin{bmatrix} \alpha & \beta \\ \beta & \alpha \end{bmatrix} \begin{bmatrix} C_L \\ C_R \end{bmatrix} = \varepsilon \begin{bmatrix} S & 0 \\ 0 & S \end{bmatrix} \begin{bmatrix} C_L \\ C_R \end{bmatrix}$$

which is sometimes written as

$$\begin{bmatrix} \alpha - \varepsilon & \beta - \varepsilon S \\ \beta - \varepsilon S & \alpha - \varepsilon \end{bmatrix} \begin{bmatrix} C_L \\ C_R \end{bmatrix} = \begin{bmatrix} 0 \\ 0 \end{bmatrix}$$

These equations reduce with the assumption of zero overlap to

$$\begin{bmatrix} \alpha & \beta \\ \beta & \alpha \end{bmatrix} \begin{bmatrix} C_L \\ C_R \end{bmatrix} = \varepsilon \begin{bmatrix} 1 & 0 \\ 0 & 1 \end{bmatrix} \begin{bmatrix} C_L \\ C_R \end{bmatrix}$$

The α parameters are identical if the two AOs χ_a and χ_b are identical, as would be the case for bonding between the two 1s orbitals of two H atoms or two $2p_\pi$ orbitals of two C atoms or two 3s orbitals of two Na atoms. If the left and right orbitals were not identical (e.g., for bonding in HeH^+ or for the π bonding in a C-O group), their α values would be different and the Hückel matrix problem would look like:

$$\begin{bmatrix} \alpha & \beta \\ \beta & \alpha' \end{bmatrix} \begin{bmatrix} C_L \\ C_R \end{bmatrix} = \varepsilon \begin{bmatrix} 1 & S \\ S & 1 \end{bmatrix} \begin{bmatrix} C_L \\ C_R \end{bmatrix}$$

To find the MO energies that result from combining the AOs, one must find the values of ε for which the above equations are valid. Taking the 2x2 matrix consisting of ε

times the overlap matrix to the left hand side, the above set of equations reduces to the third set displayed earlier. It is known from matrix algebra that such a set of linear homogeneous equations (i.e., having zeros on the right hand sides) can have non-trivial solutions (i.e., values of C that are not simply zero) only if the determinant of the matrix on the left side vanishes. Setting this determinant equal to zero gives a quadratic equation in which the ε values are the unknowns:

$$(\alpha-\varepsilon)^2 - (\beta-\varepsilon S)^2 = 0.$$

This quadratic equation can be factored into a product

$$(\alpha - \beta - \varepsilon + \varepsilon S)(\alpha + \beta - \varepsilon - \varepsilon S) = 0$$

which has two solutions

$$\varepsilon = (\alpha + \beta)/(1 + S), \text{ and } \varepsilon = (\alpha - \beta)/(1 - S).$$

As discussed earlier, it turns out that the β values are usually negative, so the lowest energy such solution is the $\varepsilon = (\alpha + \beta)/(1 + S)$ solution, which gives the energy of the bonding MO. Notice that the energies of the bonding and anti-bonding MOs are not symmetrically displaced from the value α within this version of the Hückel model that retains orbital overlap. In fact, the bonding orbital lies less than β below α, and the antibonding MO lies more than β above α because of the 1+S and 1-S factors in the respective denominators. This asymmetric lowering and raising of the MOs relative to the energies of the constituent AOs is commonly observed in chemical bonds; that is, the antibonding orbital is more antibonding than the bonding orbital is bonding. This is another important thing to keep in mind because its effects pervade chemical bonding and spectroscopy.

Having noted the effect of inclusion of AO overlap effects in the Hückel model, I should admit that it is far more common to utilize the simplified version of the Hückel model in which the S factors are ignored. In so doing, one obtains patterns of MO orbital

energies that do not reflect the asymmetric splitting in bonding and antibonding orbitals noted above. However, this simplified approach is easier to use and offers qualitatively correct MO energy orderings. So, let's proceed with our discussion of the Hückel model in its simplified version.

To obtain the LCAO-MO coefficients corresponding to the bonding and antibonding MOs, one substitutes the corresponding α values into the linear equations

$$\begin{bmatrix} \alpha - \varepsilon & \beta \\ \beta & \alpha - \varepsilon \end{bmatrix} \begin{bmatrix} C_L \\ C_R \end{bmatrix} = \begin{bmatrix} 0 \\ 0 \end{bmatrix}$$

and solves for the C_a coefficients (actually, one can solve for all but one C_a, and then use normalization of the MO to determine the final C_a). For example, for the bonding MO, we substitute $\varepsilon = \alpha + \beta$ into the above matrix equation and obtain two equations for C_L and C_R:

$$- \beta\, C_L + \beta\, C_R = 0$$

$$\beta\, C_L - \beta\, C_R = 0.$$

These two equations are clearly not independent; either one can be solved for one C in terms of the other C to give:

$$C_L = C_R,$$

which means that the bonding MO is

$$\phi = C_L\, (\chi_L + \chi_R).$$

The final unknown, C_L, is obtained by noting that ϕ is supposed to be a normalized function $\langle \phi | \phi \rangle = 1$. Within this version of the Hückel model, in which the overlap S is neglected, the normalization of ϕ leads to the following condition:

$$1 = <\phi|\phi> = C_L{}^2 (<\chi_L|\chi_L> + <\chi_R\chi_R>) = 2\,C_L{}^2$$

with the final result depending on assuming that each χ is itself also normalized. So, finally, we know that $C_L = (1/2)^{1/2}$, and hence the bonding MO is:

$$\phi = (1/2)^{1/2} (\chi_L + \chi_R).$$

Actually, the solution of $1 = 2\,C_L{}^2$ could also have yielded $C_L = -(1/2)^{1/2}$ and then, we would have

$$\phi = -(1/2)^{1/2} (\chi_L + \chi_R).$$

These two solutions are not independent (one is just –1 times the other), so only one should be included in the list of MOs. However, either one is just as good as the other because, as shown very early in this text, all of the physical properties that one computes from a wave function depend not on ψ but on $\psi^*\psi$. So, two wave functions that differ from one another by an overall sign factor as we have here have exactly the same $\psi^*\psi$ and thus are equivalent.

In like fashion, we can substitute $\varepsilon = \alpha - \beta$ into the matrix equation and solve for the C_L can C_R values that are appropriate for the antibonding MO. Doing so, gives us:

$$\phi^* = (1/2)^{1/2} (\chi_L - \chi_R)$$

or, alternatively,

$$\phi^* = (1/2)^{1/2} (\chi_R - \chi_L).$$

Again, the fact that either expression for ϕ^* is acceptable shows a property of all solutions to any Schrödinger equations; any multiple of a solution is also a solution. In the above example, the two answers for ϕ^* differ by a multiplicative factor of (-1).

Let's try another example to practice using Hückel or tight-binding theory. In particular, I'd like you to imagine two possible structures for a cluster of three Na atoms (i.e., pretend that someone came to you and asked what geometry you think such a cluster would assume in its ground electronic state), one linear and one an equilateral triangle. Further, assume that the Na-Na distances in both such clusters are equal (i.e., that the person asking for your theoretical help is willing to assume that variations in bond lengths are not the crucial factor in determining which structure is favored). In Fig. 2.11, I shown the two candidate clusters and their 3s orbitals.
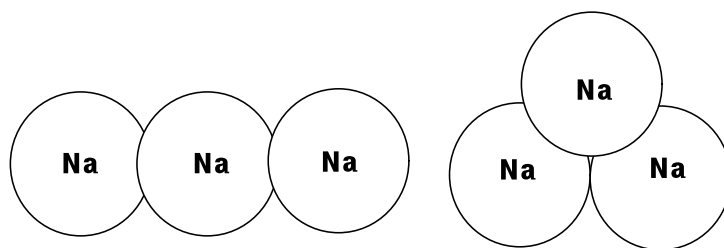
Figure 2.11. Linear and equilateral triangle structures of sodium trimer.

Numbering the three Na atoms' valence 3s orbitals χ_1, χ_2, and χ_3, we then set up the 3x3 Hückel matrix appropriate to the two candidate structures:

$$\begin{bmatrix} \alpha & \beta & 0 \\ \beta & \alpha & \beta \\ 0 & \beta & \alpha \end{bmatrix}$$

for the linear structure (n.b., the zeros arise because χ_1 and χ_3 do not overlap and thus have no β coupling matrix element). Alternatively, for the triangular structure, we find

$$\begin{bmatrix} \alpha & \beta & \beta \\ \beta & \alpha & \beta \\ \beta & \beta & \alpha \end{bmatrix}$$

as the Hückel matrix. Each of these 3x3 matrices will have three eigenvalues that we obtain by subtracting ε from their diagonals and setting the determinants of the resulting matrices to zero. For the linear case, doing so generates

$$(\alpha\text{-}\varepsilon)^3 - 2\,\beta^2(\alpha\text{-}\varepsilon) = 0,$$

and for the triangle case it produces

$$(\alpha\text{-}\varepsilon)^3 - 3\,\beta^2(\alpha\text{-}\varepsilon) + 2\,\beta^2 = 0.$$

The first cubic equation has three solutions that give the MO energies:

$$\varepsilon = \alpha + (2)^{1/2}\beta,\ \varepsilon = \alpha,\ \text{and}\ \varepsilon = \alpha - (2)^{1/2}\beta,$$

for the bonding, non-bonding and antibonding MOs, respectively. The second cubic equation also has three solutions

$$\varepsilon = \alpha + 2\beta,\ \varepsilon = \alpha - \beta\ ,\ \text{and}\ \varepsilon = \alpha - \beta.$$

So, for the linear and triangular structures, the MO energy patterns are as shown in Fig. 2.12.

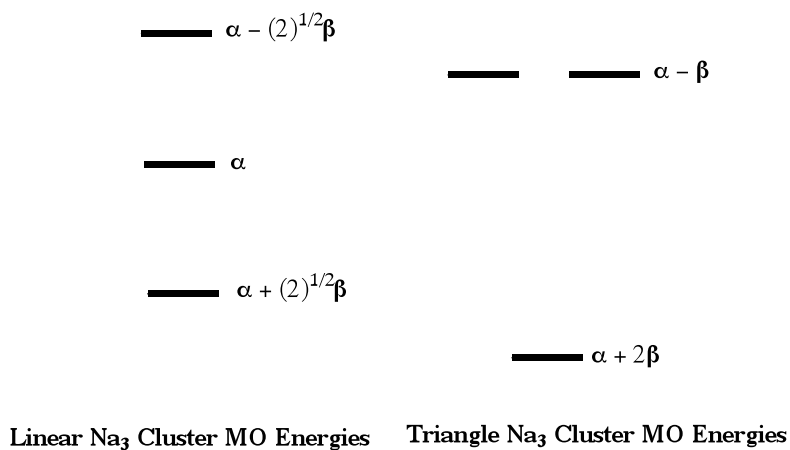Linear Na$_3$ Cluster MO Energies   Triangle Na$_3$ Cluster MO Energies

Figure 2.12. Energy orderings of molecular orbitals of linear and triangular sodium trimer.

For the neutral Na_3 cluster about which you were asked, you have three valence electrons to distribute among the lowest available orbitals. In the linear case, we place two electrons into the lowest orbital and one into the second orbital. Doing so produces a 3-electron state with a total energy of $E = 2(\alpha + 2^{1/2}\beta) + \alpha = 3\alpha + 2 \cdot 2^{1/2}\beta$. Alternatively, for the triangular species, we put two electrons into the lowest MO and one into either of the degenerate MOs resulting in a 3-electron state with total energy $E = 3\alpha + 3\beta$. Because β is a negative quantity, the total energy of the triangular structure is lower than that of the linear structure since $3 > 2 \cdot 2^{1/2}$.

The above example illustrates how we can use Hückel or tight-binding theory to make qualitative predictions (e.g., which of two shapes is likely to be of lower energy). Notice that all one needs to know to apply such a model to any set of atomic orbitals that overlap to form MOs is

(i) the individual AO energies α (which relate to the electronegativity of the AOs),

(ii) the degree to which the AOs couple (the β parameters which relate to AO overlaps),

(iii) an assumed geometrical structure whose energy one wants to estimate.

This example and the earlier example pertinent to H_2 or the π bond in ethylene also introduce the idea of symmetry. Knowing, for example, that H_2, ethylene, and linear Na_3 have a left-right plane of symmetry allows us to solve the Hückel problem in terms of symmetry-adapted atomic orbitals rather than in terms of primitive atomic orbitals as we did earlier. For example, for linear Na_3, we could use the following symmetry-adapted functions:

$$\chi_2 \text{ and } (1/2)^{1/2}\{\chi_1 + \chi_3\}$$

both of which are even under reflection through the symmetry plane and

$$(1/2)^{1/2}\{\chi_1 - \chi_3\}$$

which is odd under reflection. The 3x3 Hückel matrix would then have the form

$$\begin{bmatrix} \alpha & \sqrt{2}\beta & 0 \\ \sqrt{2}\beta & \alpha & 0 \\ 0 & 0 & \alpha \end{bmatrix}$$

For example, $H_{1,2}$ and $H_{2,3}$ are evaluated as follows

$$H_{1,2} = \langle (1/2)^{1/2} \{\chi_1 + \chi_3\}|H|\chi_2\rangle = 2(1/2)^{1/2}\beta$$

$$H_{2,3} = \langle (1/2)^{1/2} \{\chi_1 + \chi_3\}|H|\langle(1/2)^{1/2} \{\chi_1 - \chi_3\}\rangle = \tfrac{1}{2}\{ \alpha + \beta - \beta - \alpha\} = 0.$$

The three eigenvalues of the above Hückel matrix are easily seen to be α, $\alpha + \sqrt{2}\beta$, and $\alpha - \sqrt{2}\beta$, exactly as we found earlier. So, it is not necessary to go through the process of forming symmetry-adapted functions; the primitive Hückel matrix will give the correct answers even if you do not. However, using symmetry allows us to break the full (3x3 in this case) Hückel problem into separate Hückel problems for each symmetry component (one odd function and two even functions in this case, so a 1x1 and a 2x2 sub-matrix).

While we are discussing the issue of symmetry, let me briefly explain the concept of approximate symmetry again using the above Hückel problem as it applies to ethylene as an illustrative example.
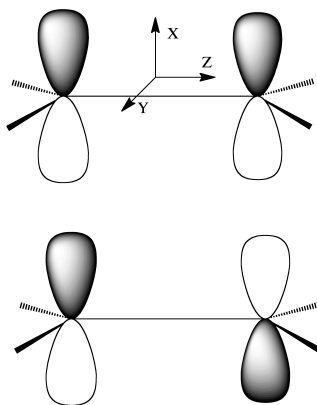

Figure 2.12a Ethylene molecule's π and π^* orbitals showing the $\sigma_{X,Y}$ reflection plane that is a symmetry property of this molecule.

Clearly, as illustrated in Fig. 2.12a, at its equilibrium geometry the ethylene molecule has a plane of symmetry (denoted $\sigma_{X,Y}$) that maps nuclei and electrons from its left to its right and vice versa. This is the symmetry element that could used to decompose the 2x2 Hückel matrix describing the π and π^* orbitals into two 1x1 matrices. However, if any of the four C-H bond lengths or HCH angles is displaced from its equilibrium value in a manner that destroys the perfect symmetry of this molecule, or if one of the C-H units were replaced by a C-CH$_3$ unit, it might appear that symmetry would no longer be a useful tool in analyzing the properties of this molecule's molecular orbitals. Fortunately, this is not the case.

Even if there is not perfect symmetry in the nuclear framework of this molecule, the two atomic p_π orbitals will combine to produce a bonding π and antibonding π^* orbital. Moreover, these two molecular orbitals will still possess nodal properties similar to those shown in Fig. 2.12a even though they will not possess perfect even and odd character relative to the $\sigma_{X,Y}$ plane. The bonding orbital will still have the same sign to the left of the $\sigma_{X,Y}$ plane as it does to the right, and the antibonding orbital will have the opposite sign to the left as it does to the right, but the magnitudes of these two orbitals will not be left-right equal. This is an example of the concept of approximate symmetry. It shows that one can use symmetry, even when it is not perfect, to predict the nodal patterns of molecular orbitals, and it is the nodal patterns that govern the relative energies of orbitals as we have seen time and again.

Let's see if you can do some of this on your own. Using the above results, would you expect the cation Na$_3^+$ to be linear or triangular? What about the anion Na$_3^-$? Next, I want you to substitute the MO energies back into the 3x3 matrix and find the C$_1$, C$_2$, and C$_3$ coefficients appropriate to each of the 3 MOs of the linear and of the triangular structure. See if doing so leads you to solutions that can be depicted as shown in Fig. 2.13, and see if you can place each set of MOs in the proper energy ordering.
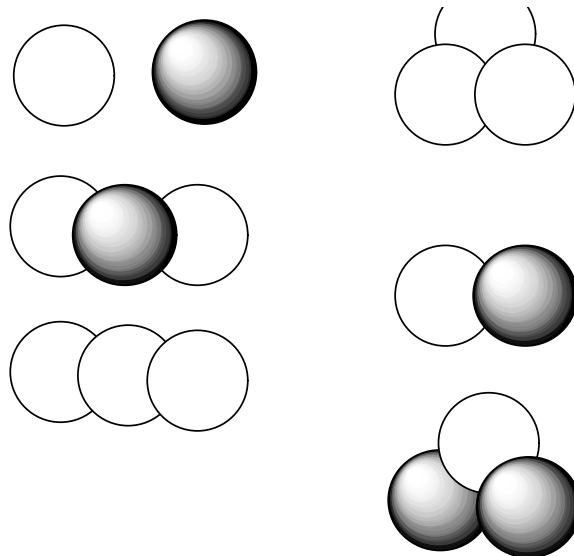
Figure 2.13. The molecular orbitals of linear and triangular sodium trimer (note, they are not energy ordered in this figure).

Now, I want to show you how to broaden your horizons and use tight-binding theory to describe all of the bonds in a more complicated molecule such as ethylene shown in Fig. 2.14. What is different about this kind of molecule when compared with metallic or conjugated species is that the bonding can be described in terms of several pairs of valence orbitals that couple to form two-center bonding and antibonding molecular orbitals. Within the Hückel model described above, each pair of orbitals that touch or overlap gives rise to a 2x2 matrix. More correctly, all n of the constituent valence orbitals form an nxn matrix, but this matrix is broken up into 2x2 blocks. Notice that this did not happen in the triangular Na_3 case where each AO touched two other AOs. For the ethlyene case, the valence orbitals consist of (a) four equivalent C sp^2 orbitals that are directed toward the four H atoms, (b) four H 1s orbitals, (c) two C sp^2 orbitals directed toward one another to form the C-C σ bond, and (d) two C p_π orbitals that will form the C-C π bond. This total of 12 orbitals generates 6 Hückel matrices as shown below the ethylene molecule.
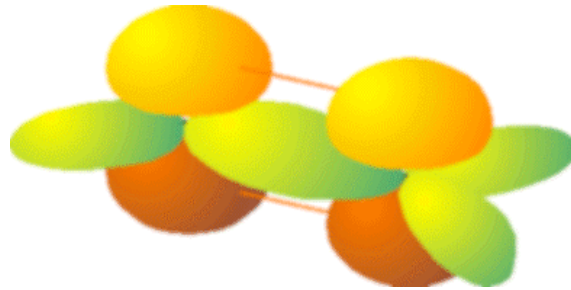
Figure 2.14 Ethylene molecule with four C-H bonds, one C-C σ bond, and one C-C π bond.

We obtain one 2x2 matrix for the C-C σ bond of the form

$$\begin{bmatrix} \alpha_{sp^2} & \beta_{sp^2,sp^2} \\ \beta_{sp^2,sp^2} & \alpha_{sp^2} \end{bmatrix}$$

and one 2x2 matrix for the C-C π bond of the form

$$\begin{bmatrix} \alpha_{p_\pi} & \beta_{p_\pi,p_\pi} \\ \beta_{p_\pi,p_\pi} & \alpha_{p_\pi} \end{bmatrix}$$

Finally, we also obtain four identical 2x2 matrices for the C-H bonds:

$$\begin{bmatrix} \alpha_{sp^2} & \beta_{sp^2,H} \\ \beta_{sp^2,H} & \alpha_H \end{bmatrix}$$

The above matrices produce (a) four identical C-H bonding MOs having energies $\varepsilon = 1/2 \{(\alpha_H + \alpha_C) - [(\alpha_H - \alpha_C)^2 + 4\beta^2]^{1/2}\}$, (b) four identical C-H antibonding MOs having energies $\varepsilon^* = 1/2 \{(\alpha_H + \alpha_C) + [(\alpha_H - \alpha_C)^2 + 4\beta^2]^{1/2}\}$, (c) one bonding C-C π orbital with $\varepsilon = \alpha_{p\pi} + \beta$, (d) a partner antibonding C-C orbital with $\varepsilon^* = \alpha_{p\pi} - \beta$, (e) a C-C σ bonding MO with $\varepsilon = \alpha_{sp2} + \beta$, and (f) its antibonding partner with $\varepsilon^* = \alpha_{sp2} - \beta$. In all of these expressions, the β parameter is supposed to be that appropriate to the specific orbitals that overlap as shown in the matrices.

If you wish to practice this exercise of breaking a large molecule down into sets of interacting valence, try to see what Hückel matrices you obtain and what bonding and antibonding MO energies you obtain for the valence orbitals of methane shown in Fig. 2.15.
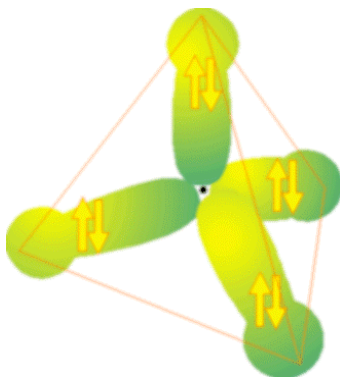
Figure 2.15. Methane molecule with four C-H bonds.

Before leaving this discussion of the Hückel/tight-binding model, I need to stress that it has its flaws (because it is based on approximations and involves neglecting certain terms in the Schrödinger equation). For example, it predicts (see above) that ethylene has four energetically identical C-H bonding MOs (and four degenerate C-H antibonding MOs). However, this is not what is seen when photoelectron spectra are used to probe the energies of these MOs. Likewise, it suggests that methane has four equivalent C-H bonding and antibonding orbitals, which, again is not true. It turns out that, in each of these two cases (ethylene and methane), the experiments indicate a grouping of four

nearly iso-energetic bonding MOs and four nearly iso-energetic antibonding MOs.
However, there is some "splitting" among these clusters of four MOs. The splittings can
be interpreted, within the Hückel model, as arising from couplings or interactions among,
for example, one sp^2 or sp^3 orbital on a given C atom and another such orbital on the
same atom. Such couplings cause the nxn Hückel matrix to not block-partition into
groups of 2x2 sub-matrices because now there exist off-diagonal β factors that couple
one pair of directed valence to another. When such couplings are included in the analysis,
one finds that the clusters of MOs expected to be degenerate are not but are split just as
the photoelectron data suggest.

2.5 Hydrogenic Orbitals

*The Hydrogenic atom problem forms the basis of much of our thinking about
atomic structure. To solve the corresponding Schrödinger equation requires separation
of the r, θ, and φ variables.*

The Schrödinger equation for a single particle of mass μ moving in a central
potential (one that depends only on the radial coordinate r) can be written as

$$- \frac{\hbar^2}{2\mu}\left(\frac{\partial^2}{\partial x^2} + \frac{\partial^2}{\partial y^2} + \frac{\partial^2}{\partial z^2}\right)\psi + V\left(\sqrt{x^2+y^2+z^2}\right)\ \psi = E\psi.$$

or, introducing the short-hand notation ∇^2:

$$- \hbar^2/2\mu\ \nabla^2\psi +\ V\ \psi = E\ \psi.$$

This equation is not separable in Cartesian coordinates (x,y,z) because of the way x,y,
and z appear together in the square root. However, it is separable in spherical coordinates
where it has the form

$$-\frac{\hbar^2}{2\mu r^2}\left(\frac{\partial}{\partial r}\left(r^2\,\frac{\partial\psi}{\partial r}\right)\right) - \frac{\hbar^2}{2\mu r^2}\frac{1}{\operatorname{Sin}\theta}\frac{\partial}{\partial\theta}\left(\operatorname{Sin}\theta\frac{\partial\psi}{\partial\theta}\right)$$

$$- \frac{\hbar^2}{2\mu r^2} \frac{1}{\sin^2\theta} \frac{\partial^2 \psi}{\partial \phi^2} + V(r)\,\psi = -\,\hbar^2/2\mu\,\nabla^2 \psi + V\,\psi = E\psi\ .$$

Subtracting $V(r)\,\psi$ from both sides of the equation and multiplying by $-\dfrac{2\mu r^2}{\hbar^2}$ then

moving the derivatives with respect to r to the right-hand side, one obtains

$$\frac{1}{\sin\theta} \frac{\partial}{\partial\theta}\left(\sin\theta \frac{\partial\psi}{\partial\theta}\right) + \frac{1}{\sin^2\theta} \frac{\partial^2\psi}{\partial\phi^2}$$

$$= -\frac{2\mu r^2}{\hbar^2}\left(E - V(r)\right)\psi - \frac{\partial}{\partial r}\left(r^2 \frac{\partial\psi}{\partial r}\right)\ .$$

Notice that, except for ψ itself, the right-hand side of this equation is a function of r only; it contains no θ or ϕ dependence. Let's call the entire right hand side $F(r)\,\psi$ to emphasize this fact.

To further separate the θ and ϕ dependence, we multiply by $\sin^2\theta$ and subtract the θ derivative terms from both sides to obtain

$$\frac{\partial^2\psi}{\partial\phi^2} = F(r)\Psi\sin^2\theta - \sin\theta\,\frac{\partial}{\partial\theta}\left(\sin\theta \frac{\partial\psi}{\partial\theta}\right).$$

Now we have separated the ϕ dependence from the θ and r dependence. We now introduce the procedure used to separate variables in differential equations and assume ψ can be written as a function of ϕ times a function of r and θ: $\psi = \Phi(\phi)\,Q(r,\theta)$. Dividing by ΦQ, we obtain

$$\frac{1}{\Phi} \frac{\partial^2 \Phi}{\partial \phi^2} = \frac{1}{Q}\left(F(r)Sin^2\theta Q - Sin\theta \frac{\partial}{\partial \theta}\left(Sin\theta \frac{\partial Q}{\partial \theta}\right)\right).$$

Now all of the ϕ dependence is isolated on the left hand side; the right hand side contains only r and θ dependence.

Whenever one has isolated the entire dependence on one variable as we have done above for the ϕ dependence, one can easily see that the left and right hand sides of the equation must equal a constant. For the above example, the left hand side contains no r or θ dependence and the right hand side contains no ϕ dependence. Because the two sides are equal for all values of r, θ, and ϕ, they both must actually be independent of r, θ, and ϕ dependence; that is, they are constant. This again is what is done when one employs the separations of variables method in partial differential equations.

For the above example, we therefore can set both sides equal to a so-called separation constant that we call -m^2. It will become clear shortly why we have chosen to express the constant in the form of minus the square of an integer. You may recall that we studied this same ϕ - equation earlier and learned how the integer m arises via. the boundary condition that ϕ and $\phi + 2\pi$ represent identical geometries.

2.5.1. The Φ Equation

The resulting Φ equation reads (the " symbol is used to represent second derivative)

$$\Phi'' + m^2\Phi = 0.$$

This equation should be familiar because it is the equation that we treated much earlier when we discussed z-component of angular momentum. So, its further analysis should also be familiar, but for completeness, I repeat much of it. The above equation has as its

most general solution

$$\Phi = A\ e^{im\phi} + B\ e^{-im\phi}\ .$$

Because the wave functions of quantum mechanics represent probability densities, they must be continuous and single-valued. The latter condition, applied to our Φ function, means (n.b., we used this in our earlier discussion of z-component of angular momentum) that

$$\Phi(\phi) = \Phi(2\pi + \phi) \qquad \text{or,}$$

$$Ae^{im\phi}\left(1 - e^{2im\pi}\right) + Be^{-im\phi}\left(1 - e^{-2im\pi}\right) = 0.$$

This condition is satisfied only when the separation constant is equal to an integer $m = 0$, $\pm 1, \pm 2, \ldots$. and provides another example of the rule that quantization comes from the boundary conditions on the wave function. Here m is restricted to certain discrete values because the wave function must be such that when you rotate through 2π about the z-axis, you must get back what you started with.

2.5.2. The Θ Equation

Now returning to the equation in which the ϕ dependence was isolated from the r and θ dependence and rearranging the θ terms to the left-hand side, we have

$$\frac{1}{\mathbf{Sin}\theta}\frac{\partial}{\partial\theta}\left(\mathbf{Sin}\theta\frac{\partial\mathbf{Q}}{\partial\theta}\right) - \frac{\mathbf{m^2Q}}{\mathbf{Sin^2}\theta} = F(r)Q.$$

In this equation we have separated the θ and r terms, so we can further decompose the wave function by introducing $Q = \Theta(\theta) R(r)$, which yields

$$\frac{1}{\Theta} \frac{1}{\mathbf{Sin}\theta} \frac{\partial}{\partial\theta}\left(\mathbf{Sin}\theta \frac{\partial\Theta}{\partial\theta}\right) - \frac{m^2}{\mathrm{Sin}^2\theta} = \frac{F(r)R}{R} = -\lambda,$$

where a second separation constant, $-\lambda$, has been introduced once the r and θ dependent terms have been separated onto the right and left hand sides, respectively.

We now can write the θ equation as

$$\frac{1}{\mathbf{Sin}\theta} \frac{\partial}{\partial\theta}\left(\mathbf{Sin}\theta \frac{\partial\Theta}{\partial\theta}\right) - \frac{m^2\Theta}{\mathrm{Sin}^2\theta} = -\lambda\,\Theta,$$

where m is the integer introduced earlier. To solve this equation for Θ, we make the substitutions $z = \mathrm{Cos}\theta$ and $P(z) = \Theta(\theta)$, so $\sqrt{1\text{-}z^2} = \mathrm{Sin}\theta$, and

$$\frac{\partial}{\partial\theta} = \frac{\partial\mathbf{z}}{\partial\theta}\frac{\partial}{\partial\mathbf{z}} = -\mathrm{Sin}\theta\,\frac{\partial}{\partial\mathbf{z}}.$$

The range of values for θ was $0 \le \theta < \pi$, so the range for z is $-1 < z < 1$. The equation for Θ, when expressed in terms of P and z, becomes

$$\frac{\mathbf{d}}{\mathbf{dz}}\left((1-\mathbf{z}^2)\frac{\mathbf{dP}}{\mathbf{dz}}\right) - \frac{m^2P}{1\text{-}z^2} + \lambda P = 0.$$

Now we can look for polynomial solutions for P, because z is restricted to be less than

unity in magnitude. If $m = 0$, we first let

$$P = \sum_{k=0} a_k z^k ,$$

and substitute into the differential equation to obtain

$$\sum_{k=0} (k+2)(k+1) a_{k+2} z^k - \sum_{k=0} (k+1)k\, a_k z^k + \lambda \sum_{k=0} a_k z^k = 0.$$

Equating like powers of z gives

$$a_{k+2} = \frac{a_k(k(k+1)-\lambda)}{(k+2)(k+1)} .$$

Note that for large values of k

$$\frac{a_{k+2}}{a_k} \to \frac{k^2\left(1+\frac{1}{k}\right)}{k^2\left(1+\frac{2}{k}\right)\left(1+\frac{1}{k}\right)} = 1.$$

Since the coefficients do not decrease with k for large k, this series will diverge for $z = \pm 1$ unless it truncates at finite order. This truncation only happens if the separation constant λ obeys $\lambda = l(l+1)$, where l is an integer (you can see this from the recursion relation giving a_{k+2} in terms of a_k; only for certain values of λ will the numerator vanish). So, once again, we see that a boundary condition (i.e., that the wave function not diverge and thus be normalizable in this case) give rise to quantization. In this case, the values of λ are restricted to $l(l+1)$; before, we saw that m is restricted to $0, \pm 1, \pm 2, \dots$.

Since the above recursion relation links every other coefficient, we can choose to solve for the even and odd functions separately. Choosing a_0 and then determining all of the even a_k in terms of this a_0, followed by rescaling all of these a_k to make the function

normalized generates an even solution. Choosing a_1 and determining all of the odd a_k in like manner, generates an odd solution.

For l= 0, the series truncates after one term and results in $P_o(z) = 1$. For l= 1 the same thing applies and $P_1(z) = z$. For l= 2, $a_2 = -6 \dfrac{a_o}{2} = -3a_o$, so one obtains $P_2 = 3z^2-1$, and so on. These polynomials are called Legendre polynomials and are denoted $P_l(z)$.

For the more general case where m $\neq$ 0, one can proceed as above to generate a polynomial solution for the Θ function. Doing so, results in the following solutions:

$$P_l^m(z) = (1 - z^2)^{|m|/2} \frac{d^{|m|} P_l(z)}{dz^{|m|}}$$

These functions are called Associated Legendre polynomials, and they constitute the solutions to the Θ problem for non-zero m values.

The above P and $e^{im\phi}$ functions, when re-expressed in terms of θ and ϕ, yield the full angular part of the wave function for any centrosymmetric potential. These solutions are usually written as

$$Y_{1,m}(\theta,\phi) = P_l^m(\cos\theta)(2\pi)^{-1/2} \exp(im\phi),$$

and are called spherical harmonics. They provide the angular solution of the r,θ, ϕ Schrödinger equation for <u>any</u> problem in which the potential depends only on the radial coordinate. Such situations include all one-electron atoms and ions (e.g., H, He^+, Li^{++}, etc.), the rotational motion of a diatomic molecule (where the potential depends only on bond length r), the motion of a nucleon in a spherically symmetrical box (as occurs in the shell model of nuclei), and the scattering of two atoms (where the potential depends only on interatomic distance).

The $Y_{1,m}$ functions possess varying number of angular nodes, which, as noted

earlier, give clear signatures of the angular or rotational energy content of the wave function. These angular nodes originate in the oscillatory nature of the Legendre and associated Legendre polynomials $P_l^m(\cos\theta)$; the higher l is, the more sign changes occur within the polynomial.

2.5.3. The R Equation

Let us now turn our attention to the radial equation, which is the only place that the explicit form of the potential appears. Using our earlier results for the equation obeyed by the R(r) function and specifying V(r) to be the Coulomb potential appropriate for an electron in the field of a nucleus of charge +Ze, yields:

$$\frac{1}{\mathbf{r}^2}\frac{\mathbf{d}}{\mathbf{dr}}\left(\mathbf{r}^2\frac{\mathbf{dR}}{\mathbf{dr}}\right)+\left(\frac{2\mu}{\hbar^2}\left(\mathbf{E}+\frac{\mathbf{Ze}^2}{\mathbf{r}}\right)-\frac{L(L+1)}{\mathbf{r}^2}\right)\mathbf{R}=0.$$

We can simplify things considerably if we choose rescaled length and energy units because doing so removes the factors that depend on μ, $\hbar$, and e. We introduce a new radial coordinate ρ and a quantity σ as follows:

$$\rho = r\left(\frac{-8\mu E}{\hbar^2}\right)^{1/2} \text{ and } \sigma = \frac{\mu \mathbf{Ze}^2}{\hbar\sqrt{-2\mu\mathbf{E}}}.$$

Notice that if E is negative, as it will be for bound states (i.e., those states with energy below that of a free electron infinitely far from the nucleus and with zero kinetic energy), ρ and σ are real. On the other hand, if E is positive, as it will be for states that lie in the continuum, ρ and σ will be imaginary. These two cases will give rise to qualitatively different behavior in the solutions of the radial equation developed below.

We now define a function S such that $S(\rho) = R(r)$ and substitute S for R to obtain:

$$\frac{1}{\rho^2}\frac{d}{d\rho}\left(\rho^2\frac{dS}{d\rho}\right) + \left(-\frac{1}{4} - \frac{L(L+1)}{\rho^2} + \frac{\sigma}{\rho}\right)S = 0.$$

The differential operator terms can be recast in several ways using

$$\frac{1}{\rho^2}\frac{d}{d\rho}\left(\rho^2\frac{dS}{d\rho}\right) = \frac{d^2S}{d\rho^2} + \frac{2}{\rho}\frac{dS}{d\rho} = \frac{1}{\rho}\frac{d^2}{d\rho^2}(\rho S).$$

The strategy that we now follow is characteristic of solving second order differential equations. We will examine the equation for S at large and small ρ values. Having found solutions at these limits, we will use a power series in ρ to interpolate between these two limits.

Let us begin by examining the solution of the above equation at small values of ρ to see how the radial functions behave at small r. As $\rho \rightarrow 0$, the term $-L(L+1)/\rho^2$ will dominate over $-1/4 + \sigma/\rho$. Neglecting these other two terms, we find that, for small values of ρ (or r), the solution should behave like ρ^L and because the function must be normalizable, we must have $L \geq 0$. Since l can be any non-negative integer, this suggests the following more general form for $S(\rho)$:

$$S(\rho) \approx \rho^L e^{-a\rho}.$$

This form will insure that the function is normalizable since $S(\rho) \rightarrow 0$ as $r \rightarrow \infty$ for all L, as long as ρ is a real quantity. If ρ is imaginary, such a form may not be normalized (see below for further consequences).

Turning now to the behavior of S for large ρ, we make the substitution of $S(\rho)$ into the above equation and keep only the terms with the largest power of ρ (i.e., the $-1/4$ term) and we allow the derivatives in the above differential equation to act on $\approx \rho^L e^{-a\rho}$. Upon so doing, we obtain the equation

$$a^2 \rho^L e^{-a\rho} = \frac{1}{4} \rho^L e^{-a\rho} \, ,$$

which leads us to conclude that the exponent in the large-ρ behavior of S is $a = \frac{1}{2}$.

Having found the small-ρ and large-ρ behaviors of $S(\rho)$, we can take S to have the following form to interpolate between large and small ρ-values:

$$S(\rho) = \rho^L e^{-\frac{\rho}{2}} \, P(\rho),$$

where the function P is expanded in an infinite power series in ρ as $P(\rho) = \sum a_k \rho^k$. Again substituting this expression for S into the above equation we obtain

$$P''\rho + P'(2L+2-\rho) + P(\sigma-L-1) = 0,$$

and then substituting the power series expansion of P and solving for the a_k's we arrive at a recursion relation for the a_k coefficients:

$$a_{k+1} = \frac{(\mathbf{k} - \sigma + L + \mathbf{1})\mathbf{a_k}}{(\mathbf{k+1})(\mathbf{k+2}L+\mathbf{2})} \, .$$

For large k, the ratio of expansion coefficients reaches the limit $\frac{a_{k+1}}{a_k} = \frac{1}{k}$, which, when substituted into $\sum a_k \rho^k$, gives the same behavior as the power series expansion of e^ρ. Because the power series expansion of P describes a function that behaves like e^ρ for

large ρ, the resulting S(ρ) function would not be normalizable because the $e^{-\frac{\rho}{2}}$ factor would be overwhelmed by this e^{ρ} dependence. Hence, the series expansion of P must truncate in order to achieve a normalizable S function. Notice that if ρ is imaginary, as it will be if E is in the continuum, the argument that the series must truncate to avoid an exponentially diverging function no longer applies. Thus, we see a key difference between bound (with ρ real) and continuum (with ρ imaginary) states. In the former case, the boundary condition of non-divergence arises; in the latter, it does not because exp(ρ/2) does not diverge if ρ is imaginary.

To truncate at a polynomial of order n', we must have n' - σ + L+ l= 0. This implies that the quantity σ introduced previously is restricted to σ = n' + L + 1, which is certainly an integer; let us call this integer n. If we label states in order of increasing n = 1,2,3,... , we see that doing so is consistent with specifying a maximum order (n') in the P(ρ) polynomial n' = 0,1,2,... after which the L-value can run from L = 0, in steps of unity up to L = n-1.

Substituting the integer n for σ, we find that the energy levels are quantized because σ is quantized (equal to n):

$$E = -\,\frac{\mu Z^2 e^4}{2\hbar^2 n^2}$$

and the scaled distance turns out to be

$$\rho = \frac{Zr}{a_o n}\,.$$

Here, the length a_o is the so-called Bohr radius $\left(a_o = \dfrac{\hbar^2}{\mu e^2}\right)$, which turns out to be 0.529 Å; it appears once the above E-expression is substituted into the equation for ρ. Using the recursion equation to solve for the polynomial's coefficients a_k for any choice of n

and L quantum numbers generates a so-called Laguerre polynomial; $P_{n-L-1}(\rho)$. They contain powers of ρ from zero through n-L-1, and they have n-L-1 sign changes as the radial coordinate ranges from zero to infinity. It is these sign changes in the Laguerre polynomials that cause the radial parts of the hydrogenic wave functions to have n-L-1 nodes. For example, 3d orbitals have no radial nodes, but 4d orbitals have one; and, as shown in Fig. 2.16, 3p orbitals have one while 3s orbitals have two. Once again, the higher the number of nodes, the higher the energy in the radial direction.
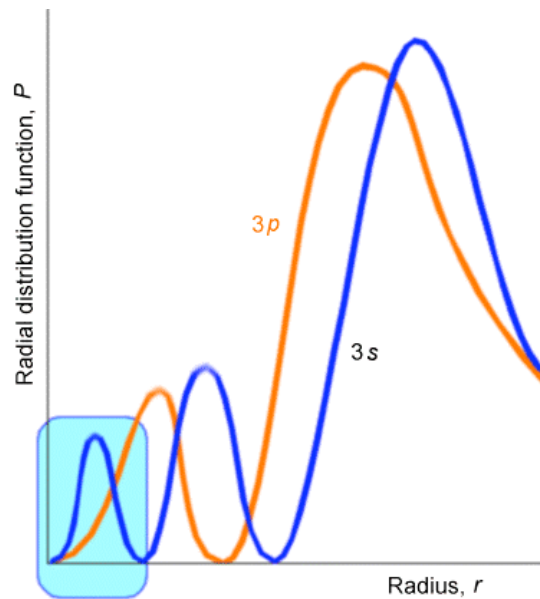

Figure 2.16. Plots of the probability densities $r^2|R(r)|^2$ of the radial parts of the 3s and 3p orbitals

Let me again remind you about the danger of trying to understand quantum wave functions or probabilities in terms of classical dynamics. What kind of potential V(r) would give rise to, for example, the 3s P(r) plot shown above? Classical mechanics suggests that P should be large where the particle moves slowly and small where it moves quickly. So, the 3s P(r) plot suggests that the radial speed of the electron has three regions where it is low (i.e., where the peaks in P are) and two regions where it is very large (i.e., where the nodes are). This, in turn, suggests that the radial potential V(r) experienced by

the 3s electron is high in three regions (near peaks in P) and low in two regions. Of course, this conclusion about the form of V(r) is nonsense and again illustrates how one must not be drawn into trying to think of the classical motion of the particle, especially for quantum states with small quantum number. In fact, the low quantum number states of such one-electron atoms and ions have their radial P(r) plots focused in regions of r-space where the potential $-Ze^2/r$ is most attractive (i.e., largest in magnitude).

Finally, we note that the energy quantization does not arise for states lying in the continuum because the condition that the expansion of P(ρ) terminate does not arise. The solutions of the radial equation appropriate to these scattering states (which relate to the scattering motion of an electron in the field of a nucleus of charge Z) are a bit outside the scope of this text, so we will not treat them further here. For the interested student, they are treated on p. 90 of the text by Eyring, Walter, and Kimball to which I refer in the Introductory Remarks to this text.

To review, separation of variables has been used to solve the full r,θ,ϕ Schrödinger equation for one electron moving about a nucleus of charge Z. The θ and ϕ solutions are the spherical harmonics $Y_{L,m}(\theta,\phi)$. The bound-state radial solutions

$$R_{n,L}(r) = S(\rho) = \rho^L e^{-\frac{\rho}{2}} P_{n-L-1}(\rho)$$

depend on the n and L quantum numbers and are given in terms of the Laguerre polynomials.

2.5.4. Summary

To summarize, the quantum numbers L and m arise through boundary conditions requiring that $\psi(\theta)$ be normalizable (i.e., not diverge) and $\psi(\phi) = \psi(\phi+2\pi)$. The radial equation, which is the only place the potential energy enters, is found to possess both bound-states (i.e., states whose energies lie below the asymptote at which the potential vanishes and the kinetic energy is zero) and continuum states lying energetically above this asymptote. The former states are spatially confined by the potential, but the latter are not. The resulting hydrogenic wave functions (angular and radial) and energies are

summarized on pp. 133-136 in the text by L. Pauling and E. B. Wilson for n up to and including 6 and L up to 5 (i.e, for s, p, d, f, g, and h orbitals).

There are both bound and continuum solutions to the radial Schrödinger equation for the attractive coulomb potential because, at energies below the asymptote, the potential confines the particle between r=0 and an outer classical turning point, whereas at energies above the asymptote, the particle is no longer confined by an outer turning point (see Fig. 2.17). This provides yet another example of how quantized states arise when the potential spatially confines the particle, but continuum states arise when the particle is not spatially confined.
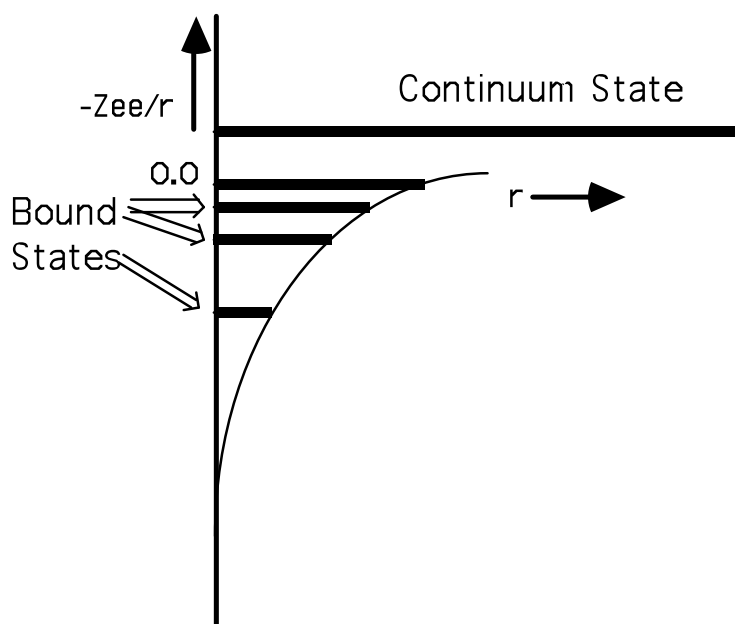

Figure 2.17. Radial Potential for Hydrogenic Atoms and Bound and Continuum Orbital Energies.

The solutions of this one-electron problem form the qualitative basis for much of atomic and molecular orbital theory. For this reason, the reader is encouraged to gain a firmer understanding of the nature of the radial and angular parts of these wave functions. The orbitals that result are labeled by n, l, and m quantum numbers for the bound states and by l and m quantum numbers and the energy E for the continuum states. Much as the

particle-in-a-box orbitals are used to qualitatively describe π- electrons in conjugated polyenes, these so-called hydrogen-like orbitals provide qualitative descriptions of orbitals of atoms with more than a single electron. By introducing the concept of screening as a way to represent the repulsive interactions among the electrons of an atom, an effective nuclear charge Z_{eff} can be used in place of Z in the $\psi_{n,l,m}$ and E_n to generate approximate atomic orbitals to be filled by electrons in a many-electron atom. For example, in the crudest approximation of a carbon atom, the two 1s electrons experience the full nuclear attraction so $Z_{eff} = 6$ for them, whereas the 2s and 2p electrons are screened by the two 1s electrons, so $Z_{eff} = 4$ for them. Within this approximation, one then occupies two 1s orbitals with Z = 6, two 2s orbitals with Z = 4 and two 2p orbitals with Z=4 in forming the full six-electron wave function of the lowest-energy state of carbon. It should be noted that the use of screened nuclear charges as just discussed is different from the use of a quantum defect parameter δ as discussed regarding Rydberg orbitals in Chapter 1. The Z = 4 screened charge for carbon's 2s and 2p orbitals is attempting to represent the effect of the inner-shell 1s electrons on the 2s and 2p orbitals. The modification of the principal quantum number made by replacing n by (n- δ) represents the penetration of the orbital with nominal quantum number n inside its inner-shells.

2.6. Electron Tunneling

Tunneling is a phenomenon of quantum mechanics, not classical mechanics. It is an extremely important subject that occurs in a wide variety of chemical species including nano-scale electronic devices and protons moving through water.

As we have seen several times already, solutions to the Schrödinger equation display several properties that are very different from what one experiences in Newtonian dynamics. One of the most unusual and important is that the particles one describes using quantum mechanics can move into regions of space where they would not be allowed to go if they obeyed classical equations. We call these classically forbidden regions. Let us consider an example to illustrate this so-called tunneling phenomenon. Specifically, we think of an electron (a particle that we likely would use quantum mechanics to describe) moving in a direction we will call R under the influence of a potential that is:

a. Infinite for $R < 0$ (this could, for example, represent a region of space within a solid material where the electron experiences very repulsive interactions with other electrons);

b. Constant and negative for some range of R between $R = 0$ and R_{max} (this could represent the attractive interaction of the electrons with those atoms or molecules in a finite region or surface of a solid);

c. Constant and repulsive (i.e., positive) by an amount $\delta V + D_e$ for another finite region from R_{max} to $R_{max} + \delta$ (this could represent the repulsive interactions between the electrons and a layer of molecules of thickness δ lying on the surface of the solid at R_{max});

d. Constant and equal to D_e from $R_{maz} + \delta$ to infinity (this could represent the electron being removed from the solid, but with a work function energy cost of D_e, and moving freely in the vacuum above the surface and the ad-layer). Such a potential is shown in Fig. 2.18.
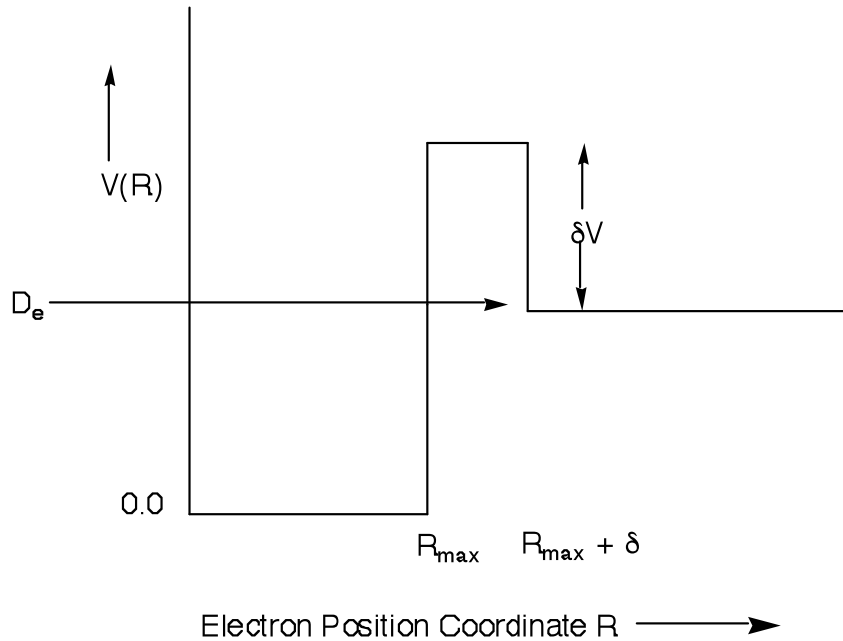

Figure 2.18. One-dimensional potential showing a well, a barrier, and the asymptotic region.

The piecewise nature of this potential allows the one-dimensional Schrödinger equation to be solved analytically. For energies lying in the range $D_e < E < D_e + \delta V$, an especially interesting class of solutions exists. These so-called resonance states occur at energies that are determined by the condition that the amplitude of the wave function within the barrier (i.e., for $0 \leq R \leq R_{max}$) be large. Let us now turn our attention to this specific energy regime, which also serves to introduce the tunneling phenomenon.

The piecewise solutions to the Schrödinger equation appropriate to the resonance case are easily written down in terms of sin and cos or exponential functions, using the following three definitions:

$$k = \sqrt{2m_e E / \hbar^2}, k' = \sqrt{2m_e(E - D_e)/\hbar^2}, \kappa' = \sqrt{2m_e(D_e + \delta V - E)/\hbar^2}$$

The combination of sin(kR) and cos(kR) that solve the Schrödinger equation in the inner region and that vanish at R=0 (because the function must vanish within the region where V is infinite and because it must be continuous, it must vanish at R=0) is:

$$\psi = A\sin(kR) \qquad \qquad (\text{for } 0 \leq R \leq R_{max}).$$

Between R_{max} and $R_{max} + \delta$, there are two solutions that obey the Schrödiger equation, so the most general solution is a combination of these two:

$$\psi = B^+ \exp(\kappa' R) + B^- \exp(-\kappa' R) \qquad (\text{for } R_{max} \leq R \leq R_{max} + \delta).$$

Finally, in the region beyond $R_{max} + \delta$, we can use a combination of either sin(k'R) and cos(k'R) or exp(ik'R) and exp(-ik'R) to express the solution. Unlike the region near R=0, where it was most convenient to use the sin and cos functions because one of them could be "thrown away" since it could not meet the boundary condition of vanishing at R=0, in this large-R region, either set is acceptable. We choose to use the exp(ik'R) and

exp(-ik'R) set because each of these functions is an eigenfunction of the momentum operator $-i\hbar\partial/\partial R$. This allows us to discuss amplitudes for electrons moving with positive momentum and with negative momentum. So, in this region, the most general solution is

$$\psi = C\ exp(ik'R) + D\ exp(-ik'R) \qquad\qquad (\text{for } R_{max} + \delta \le R < \infty).$$

There are four amplitudes (A, B_+, B_-, and C) that can be expressed in terms of the specified amplitude D of the incoming flux (e.g., pretend that we know the flux of electrons that our experimental apparatus shoots at the surface). Four equations that can be used to achieve this goal result when ψ and $d\psi/dR$ are matched at R_{max} and at $R_{max} + \delta$ (one of the essential properties of solutions to the Schrödinger equation is that they and their first derivative are continuous; these properties relate to ψ being a probability and the momentum $-ih\partial/\partial R$ being continuous). These four equations are:

$$A\sin(kR_{max}) = B^+ exp(\kappa'R_{max}) + B^- exp(-\kappa'R_{max}),$$

$$Ak\cos(kR_{max}) = \kappa'B^+ exp(\kappa'R_{max}) - \kappa'B^- exp(-\kappa'R_{max}),$$

$$B^+ exp(\kappa'(R_{max} + \delta)) + B^- exp(-\kappa'(R_{max} + \delta))$$

$$= C\ exp(ik'(R_{max} + \delta) + D\ exp(-ik'(R_{max} + \delta),$$

$$\kappa'B^+ exp(\kappa'(R_{max} + \delta)) - \kappa'B^- exp(-\kappa'(R_{max} + \delta))$$

$$= ik'C\ exp(ik'(R_{max} + \delta)) - ik'\ D\ exp(-ik'(R_{max} + \delta)).$$

It is especially instructive to consider the value of A/D that results from solving this set of four equations in four unknowns because the modulus of this ratio provides information about the relative amount of amplitude that exists inside the barrier in the attractive region of the potential compared to that existing in the asymptotic region as incoming

flux.

The result of solving for A/D is:

$$A/D = 4 \ \kappa'\exp(-ik'(R_{max}+\delta))$$

$$\{\exp(\kappa'\delta)(ik'-\kappa')(\kappa'\sin(kR_{max})+k\cos(kR_{max}))/ik'$$

$$+ \exp(-\kappa'\delta)(ik'+\kappa')(\kappa'\sin(kR_{max})-k\cos(kR_{max}))/ik' \ \}^{-1}.$$

To simplify this result in a manner that focuses on conditions where tunneling plays a key role in creating the resonance states, it is instructive to consider this result under conditions of a high (large $D_e + \delta V - E$) and thick (large δ) barrier. In such a case, the factor $\exp(-\kappa'\delta)$ will be very small compared to its counterpart $\exp(\kappa'\delta)$, and so

$$A/D = 4 \ \frac{ik'\kappa'}{ik'-\kappa'} \exp(-ik'(R_{max}+\delta)) \ \exp(-\kappa'\delta) \ \{\kappa'\sin(kR_{max})+k\cos(kR_{max}) \ \}^{-1}.$$

The $\exp(-\kappa'\delta)$ factor in A/D causes the magnitude of the wave function inside the barrier to be small in most circumstances; we say that incident flux must tunnel through the barrier to reach the inner region and that $\exp(-\kappa'\delta)$ governs the probability of this tunneling.

Keep in mind that, in the energy range we are considering ($E < D_e+\delta$), a classical particle could not even enter the region $R_{max} < R < R_{max} + \delta$; this is why we call this the classically forbidden or tunneling region. A classical particle starting in the large-R region can not enter, let alone penetrate, this region, so such a particle could never end up in the $0 < R < R_{max}$ inner region. Likewise, a classical particle that begins in the inner region can never penetrate the tunneling region and escape into the large-R region. Were it not for the fact that electrons obey a Schrödinger equation rather than Newtonian dynamics, tunneling would not occur and, for example, scanning tunneling microscopy (STM), which has proven to be a wonderful and powerful tool for imaging molecules on

and near surfaces, would not exist. Likewise, many of the devices that appear in our modern electronic tools and games, which depend on currents induced by tunneling through various junctions, would not be available. But, or course, tunneling does occur and it can have remarkable effects.

Let us examine an especially important (in chemistry) phenomenon that takes place because of tunneling and that occurs when the energy E assumes very special values. The magnitude of the A/D factor in the above solutions of the Schrödinger equation can become large if the energy E is such that the denominator in the above expression for A/D approaches zero. This happens when

$$\kappa'\sin(kR_{max})+k\cos(kR_{max})$$

or if

$$\tan(kR_{max}) = - k/\kappa'.$$

It can be shown that the above condition is similar to the energy quantization condition

$$\tan(kR_{max}) = - k/\kappa$$

that arises when bound states of a finite potential well similar to that shown above but with the barrier between R_{max} and $R_{max} + \delta$ missing and with E below D_e. There is, however, a difference. In the bound-state situation, two energy-related parameters occur

$$k = \sqrt{2\mu E/\hbar^2}$$

and

$$\kappa = \sqrt{2\mu(D_e - E)/\hbar^2} \ .$$

In the case we are now considering, k is the same, but

$$\kappa' = \sqrt{2\mu(D_e + \delta V - E)/\hbar^2} \;)$$

rather than κ occurs, so the two equations involving $\tan(kR_{max})$ are not identical, but they are quite similar.

Another observation that is useful to make about the situations in which A/D becomes very large can be made by considering the case of a very high barrier (so that κ' is much larger than k). In this case, the denominator that appears in A/D

$$\kappa'\sin(kR_{max}) + k\cos(kR_{max}) \cong \kappa' \sin(kR_{max})$$

can become small at energies satisfying

$$\sin(kR_{max}) \cong 0.$$

This condition is nothing but the energy quantization condition that occurs for the particle-in-a-box potential shown in Fig. 2.19.
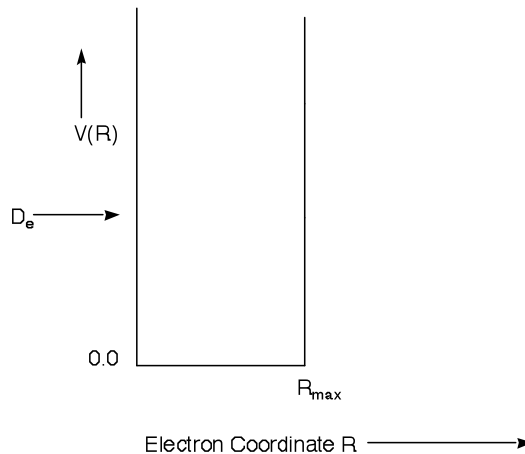

Figure 2.19. One-dimensional potential similar to the tunneling potential but without the barrier and asymptotic region.

This potential is identical to the potential that we were examining for $0 \le R \le R_{max}$, but extends to infinity beyond R_{max}; the barrier and the dissociation asymptote displayed by our potential are absent.

Let's consider what this tunneling problem has taught us. First, it showed us that quantum particles penetrate into classically forbidden regions. It showed that, at certain so-called resonance energies, tunneling is much more likely than at energies that are off-resonance. In our model problem, this means that electrons impinging on the surface with resonance kinetic energies will have a very high probability of tunneling to produce an electron that is highly localized (i.e., trapped) in the $0 < R < R_{max}$ region. Likewise, it means that an electron prepared (e.g., perhaps by photo-excitation from a lower-energy electronic state) within the $0 < R < R_{max}$ region will remain trapped in this region for a long time (i.e., will have a low probability of tunneling outward).

In the case just mentioned, it would make sense to solve the four equations for the amplitude C of the outgoing wave in the $R > R_{max}$ region in terms of the A amplitude. If we were to solve for C/A and then examine under what conditions the amplitude of this ratio would become small (so the electron cannot escape), we would find the same $\tan(kR_{max}) = -k/\kappa'$ resonance condition as we found from the other point of view. This means that the resonance energies tell us for what collision energies the electron will tunnel inward and produce a trapped electron and, at these same energies, an electron that is trapped will not escape quickly.

Whenever one has a barrier on a potential energy surface, at energies above the dissociation asymptote D_e but below the top of the barrier ($D_e + \delta V$ here), one can expect resonance states to occur at special scattering energies E. As we illustrated with the model problem, these so-called resonance energies can often be approximated by the bound-state energies of a potential that is identical to the potential of interest in the inner region ($0 \le R \le R_{max}$) but that extends to infinity beyond the top of the barrier (i.e., beyond the barrier, it does not fall back to values below E).

The chemical significance of resonances is great. Highly rotationally excited molecules may have more than enough total energy to dissociate (D_e), but this energy may be stored in the rotational motion, and the vibrational energy may be less than D_e. In

terms of the above model, high rotational angular momentum may produce a significant centrifugal barrier in the effective potential that characterizes the molecule's vibration, but the system's vibrational energy may lie significantly below D_e. In such a case, and when viewed in terms of motion on an angular-momentum-modified effective potential such as I show in Fig. 2.20 , the lifetime of the molecule with respect to dissociation is determined by the rate of tunneling through the barrier.
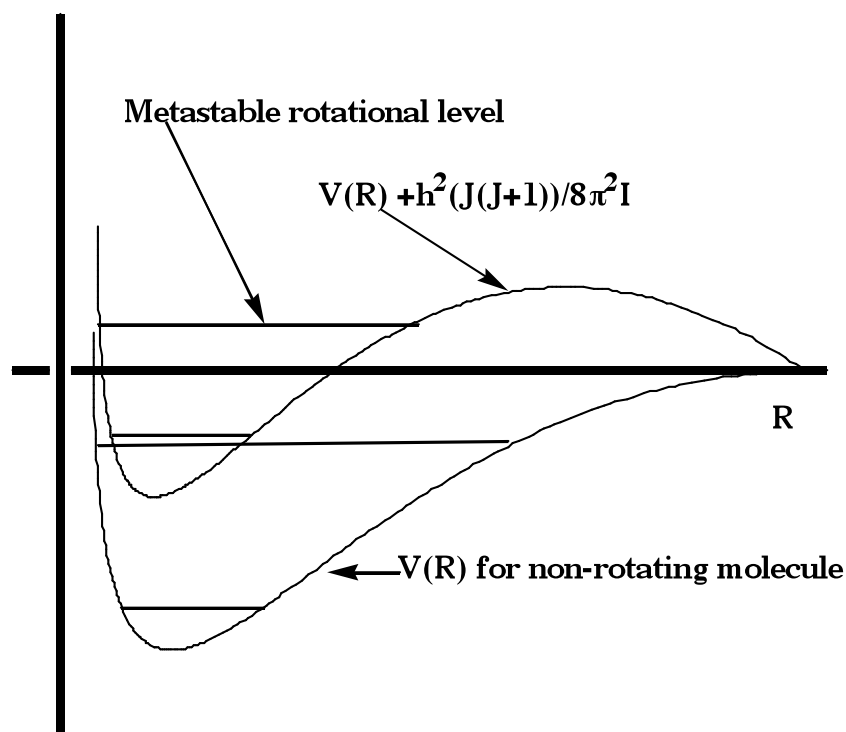

Figure 2.20. Radial potential for non-rotating ($J = 0$) molecule and for rotating molecule.

In this case, one speaks of rotational predissociation of the molecule. The lifetime τ can be estimated by computing the frequency ν at which flux that exists inside R_{max} strikes the barrier at R_{max}

$$\nu = \frac{\hbar k}{2\mu R_{max}} \quad (sec^{-1})$$

and then multiplying by the probability P that flux tunnels through the barrier from R_{max} to $R_{max} + \delta$:

$$P = \exp(-2\kappa'\delta).$$

The result is that

$$\tau^{-1} = \frac{\hbar k}{2\mu R_{max}} \exp(-2\kappa'\delta)$$

with the energy E entering into k and κ' being determined by the resonance condition: $(\kappa'\sin(kR_{max})+k\cos(kR_{max})) = $ minimum. We note that the probability of tunneling exp(-2$\kappa'\delta$) falls of exponentially with a factor depending on the width δ of the barrier through which the particle must tunnel multiplied by κ', which depends on the height of the barrier $D_e + \delta$ above the energy E available. This exponential dependence on thickness and height of the barriers is something you should keep in mind because it appears in all tunneling rate expressions.

Another important case in which tunneling occurs is in electronically metastable states of anions. In so-called shape resonance states, the anion's extra electron experiences

a. an attractive potential due to its interaction with the underlying neutral molecule's dipole, quadrupole, and induced electrostatic moments, as well as

b. a centrifugal potential of the form $L(L+1)h^2/8\pi^2 m_e R^2$ whose magnitude depends on the angular character of the orbital the extra electron occupies.

When combined, the above attractive and centrifugal potentials produce an effective radial potential of the form shown in Fig. 2.21 for the N_2^- case in which the added electron occupies the π^* orbital which has L=2 character when viewed from the center of the N-N bond. Again, tunneling through the barrier in this potential determines the lifetimes of such shape resonance states.
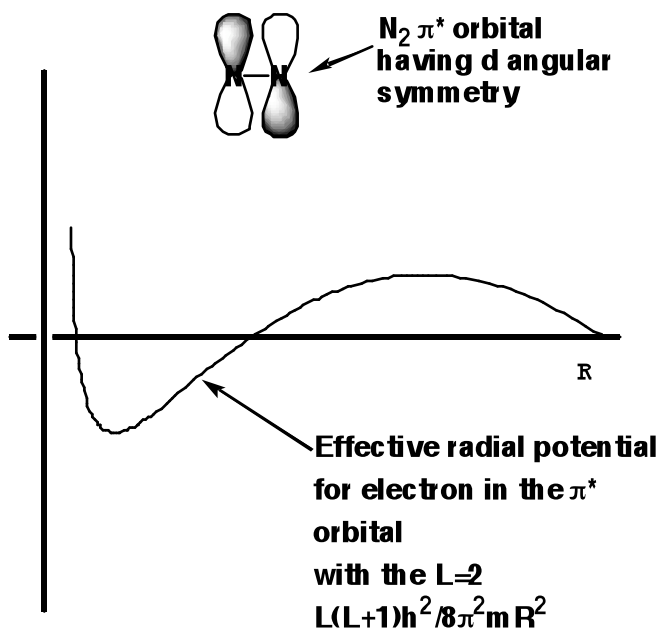
N$_2$ π* orbital having d angular symmetry

Effective radial potential for electron in the π* orbital with the L=2 L(L+1)h^2/8π^{2}m R^2

Figure 2.21 Effective radial potential for the excess electron in N$_2^-$ occupying the π* orbital which has a dominant L = 2 component.

Although the examples treated above analytically involved piecewise constant potentials (so the Schrödinger equation and the boundary matching conditions could be solved exactly), many of the characteristics observed carry over to more chemically realistic situations. In fact, one can often model chemical reaction processes in terms of motion along a reaction coordinate (s) from a region characteristic of reactant materials where the potential surface is positively curved in all direction and all forces (i.e., gradients of the potential along all internal coordinates) vanish; to a transition state at which the potential surface's curvature along s is negative while all other curvatures are positive and all forces vanish; onward to product materials where again all curvatures are positive and all forces vanish. A prototypical trace of the energy variation along such a reaction coordinate is in Fig. 2.22.
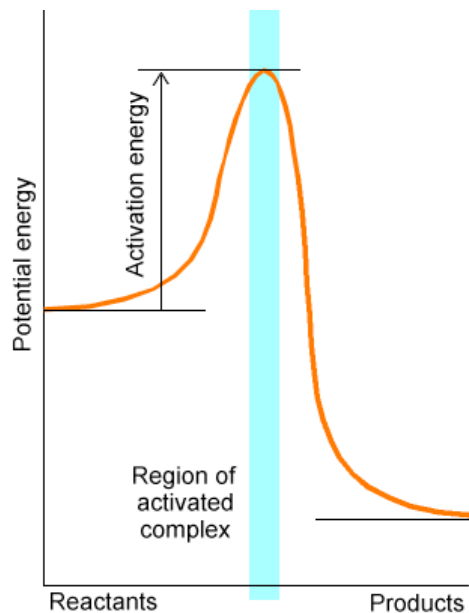
Figure 2.22. Energy profile along a reaction path showing the barrier through which tunneling may occur.

Near the transition state at the top of the barrier on this surface, tunneling through the barrier plays an important role if the masses of the particles moving in this region are sufficiently light. Specifically, if H or D atoms are involved in the bond breaking and forming in this region of the energy surface, tunneling must usually be considered in treating the dynamics.

Within the above reaction path point of view, motion transverse to the reaction coordinate is often modeled in terms of local harmonic motion although more sophisticated treatments of the dynamics is possible. This picture leads one to consider motion along a single degree of freedom, with respect to which much of the above treatment can be carried over, coupled to transverse motion along all other internal degrees of freedom taking place under an entirely positively curved potential (which therefore produces restoring forces to movement away from the streambed traced out by the reaction path). This point of view constitutes one of the most widely used and successful models of molecular reaction dynamics and is treated in more detail in Chapters 3 and 8 of this text.

2.7. Angular Momentum

2.7.1. Orbital Angular Momentum

A particle moving with momentum **p** at a position **r** relative to some coordinate origin has so-called orbital angular momentum equal to **L** = **r** x **p** . The three components of this angular momentum vector in a Cartesian coordinate system located at the origin mentioned above are given in terms of the Cartesian coordinates of **r** and **p** as follows:

$$L_z = x\, p_y - y\, p_x ,$$

$$L_x = y\, p_z - z\, p_y ,$$

$$L_y = z\, p_x - x\, p_z .$$

Using the fundamental commutation relations among the Cartesian coordinates and the Cartesian momenta:

$$[q_k, p_j] = q_k\, p_j - p_j\, q_k = i\hbar\, \delta_{j,k}\ (\ j,k = x,y,z) ,$$

which are proven by considering quantities of the from

$$(xp_x - p_x x)f = -i\hbar[x\frac{\partial f}{\partial x} - \frac{\partial (xf)}{\partial x}] = i\hbar f ,$$

it can be shown that the above angular momentum operators obey the following set of commutation relations:

$$[L_x, L_y] = i\hbar\, L_z ,$$

$$[L_y, L_z] = i\hbar\, L_x ,$$

$$[L_z, L_x] = i\hbar\, L_y .$$

Although the components of **L** do not commute with one another, they can be shown to commute with the operator L^2 defined by

$$L^2 = L_x{}^2 + L_y{}^2 + L_z{}^2 \ .$$

This new operator is referred to as the square of the total angular momentum operator.

The commutation properties of the components of **L** allow us to conclude that complete sets of functions can be found that are eigenfunctions of L^2 and of one, but not more than one, component of **L**. It is convention to select this one component as L_z, and to label the resulting simultaneous eigenstates of L^2 and L_z as |l,m> according to the corresponding eigenvalues:

$$L^2 \ |l,m> = \hbar^2 \ l(l+1) \ |l,m>, l = 0,1,2,3,....$$

$$L_z \ |l,m> = \hbar \ m \ |l,m>, m = \pm \ l, \pm(l-1), \pm(l-2), ... \pm(l-(l-1)), 0.$$

These eigenfunctions of L^2 and of L_z will not, in general, be eigenfunctions of either L_x or of L_y. This means that any measurement of L_x or L_y will necessarily change the wave function if it begins as an eigenfunction of L_z.

The above expressions for L_x, L_y, and L_z can be mapped into quantum mechanical operators by substituting x, y, and z as the corresponding coordinate operators and $-i\hbar\partial/\partial x$, $-i\hbar\partial/\partial y$, and $-i\hbar\partial/\partial z$ for p_x, p_y, and p_z, respectively. The resulting operators can then be transformed into spherical coordinates the results of which are:

$$L_z = -i\hbar \ \partial/\partial\phi \ ,$$

$$L_x = i\hbar \ \{\sin\phi \ \partial/\partial\theta + \cot\theta \ \cos\phi \ \partial/\partial\phi\} \ ,$$

$$L_y = -i\hbar \ \{\cos\phi \ \partial/\partial\theta - \cot\theta \ \sin\phi \ \partial/\partial\phi\} \ ,$$

$$L^2 = -\hbar^2 \{(1/\sin\theta) \, \partial/\partial\theta \, (\sin\theta \, \partial/\partial\theta) + (1/\sin^2\theta) \, \partial^2/\partial\phi^2\} \, .$$

2.7.2. Properties of General Angular Momenta

There are many types of angular momenta that one encounters in chemistry. Orbital angular momenta, such as that introduced above, arise in electronic motion in atoms, in atom-atom and electron-atom collisions, and in rotational motion in molecules. Intrinsic spin angular momentum is present in electrons, H^1, H^2, C^{13}, and many other nuclei. In this Section, we will deal with the behavior of any and all angular momenta and their corresponding eigenfunctions.

At times, an atom or molecule contains more than one type of angular momentum. The Hamiltonian's interaction potentials present in a particular species may or may not cause these individual angular momenta to be coupled to an appreciable extent (i.e., the Hamiltonian may or may not contain terms that refer simultaneously to two or more of these angular momenta). For example, the NH$^-$ ion, which has a $^2\Pi$ ground electronic state (its electronic configuration is $1s_N^2 2\sigma^2 3\sigma^2 2p_{\pi x}^2 2p_{\pi y}^1$) has electronic spin, electronic orbital, and molecular rotational angular momenta. The full Hamiltonian H contains terms that couple the electronic spin and orbital angular momenta, thereby causing them individually to not commute with H.

In such cases, the eigenstates of the system can be labeled rigorously only by angular momentum quantum numbers j and m belonging to the total angular momentum operators J^2 and J_z. The total angular momentum of a collection of individual angular momenta is defined, component-by-component, as follows:

$$J_k = \Sigma_i \, J_k(i),$$

where k labels x, y, and z, and i labels the constituents whose angular momenta couple to produce **J**.

For the remainder of this Section, we will study eigenfunction-eigenvalue

relationships that are characteristic of all angular momenta and which are consequences of the commutation relations among the angular momentum vector's three components. We will also study how one combines eigenfunctions of two or more angular momenta {**J**(i)} to produce eigenfunctions of the total **J**.

a. Consequences of the Commutation Relations

Any set of three operators that obey

$$[J_x, J_y] = i\hbar J_z ,$$

$$[J_y, J_z] = i\hbar J_x ,$$

$$[J_z, J_x] = i\hbar J_y ,$$

will be taken to define an angular momentum **J**, whose square $J^2 = J_x^2 + J_y^2 + J_z^2$ commutes with all three of its components. It is useful to also introduce two combinations of the three fundamental operators J_x and J_y:

$$J_\pm = J_x \pm i J_y ,$$

and to refer to them as raising and lowering operators for reasons that will be made clear below. These new operators can be shown to obey the following commutation relations:

$$[J^2, J_\pm] = 0,$$

$$[J_z, J_\pm] = \pm \hbar J_\pm .$$

Using only the above commutation properties, it is possible to prove important properties of the eigenfunctions and eigenvalues of J^2 and J_z. Let us assume that we have

found a set of simultaneous eigenfunctions of J^2 and J_z ; the fact that these two operators commute tells us that this is possible. Let us label the eigenvalues belonging to these functions:

$$J^2 \; |j,m\rangle = \hbar^2 \; f(j,m) \; |j,m\rangle,$$

$$J_z \; |j,m\rangle = \hbar \; m \; |j,m\rangle,$$

in terms of the quantities m and $f(j,m)$. Although we certainly hint that these quantities must be related to certain j and m quantum numbers, we have not yet proven this, although we will soon do so. For now, we view $f(j,m)$ and m simply as symbols that represent the respective eigenvalues. Because both J^2 and J_z are Hermitian, eigenfunctions belonging to different $f(j,m)$ or m quantum numbers must be orthogonal:

$$\langle j,m|j',m'\rangle = \delta_{m,m'} \; \delta_{j,j'} \; .$$

We now prove several identities that are needed to discover the information about the eigenvalues and eigenfunctions of general angular momenta that we are after. Later in this Section, the essential results are summarized.

i. There is a Maximum and a Minimum Eigenvalue for J_z

Because all of the components of **J** are Hermitian, and because the scalar product of any function with itself is positive semi-definite, the following identity holds:

$$\langle j,m|J_x^2 + J_y^2|j,m\rangle = \langle J_x\langle j,m| \; J_x|j,m\rangle + \langle J_y\langle j,m| \; J_y|j,m\rangle \; \geq 0.$$

However, $J_x^2 + J_y^2$ is equal to $J^2 - J_z^2$, so this inequality implies that

$$\langle j,m| \; J^2 - J_z^2 \; |j,m\rangle = \hbar^2 \; \{f(j,m) - m^2\} \geq 0,$$

which, in turn, implies that m^2 must be less than or equal to $f(j,m)$. Hence, for any value of the total angular momentum eigenvalue f, the z-projection eigenvalue (m) must have a maximum and a minimum value and both of these must be less than or equal to the total angular momentum squared eigenvalue f.

ii. The Raising and Lowering Operators Change the J_z Eigenvalue but not the J^2 Eigenvalue When Acting on |j,m>

Applying the commutation relations obeyed by $J_\pm$ to |j,m> yields another useful result:

$$J_z J_\pm |j,m> - J_\pm J_z |j,m> = \pm \hbar J_\pm |j,m>,$$

$$J^2 J_\pm |j,m> - J_\pm J^2 |j,m> = 0.$$

Now, using the fact that |j,m> is an eigenstate of J^2 and of J_z, these identities give

$$J_z J_\pm |j,m> = (m\hbar \pm \hbar) J_\pm |j,m> = \hbar (m\pm1) |j,m>,$$

$$J^2 J_\pm |j,m> = \hbar^2 f(j,m) J_\pm |j,m>.$$

These equations prove that the functions $J_\pm$ |j,m> must either themselves be eigenfunctions of J^2 and J_z, with eigenvalues $\hbar^2 f(j,m)$ and $\hbar (m+1)$, respectively, or $J_\pm$ |j,m> must equal zero. In the former case, we see that $J_\pm$ acting on |j,m> generates a new eigenstate with the same J^2 eigenvalue as |j,m> but with one unit of $\hbar$ higher or lower in J_z eigenvalue. It is for this reason that we call $J_\pm$ raising and lowering operators. Notice that, although $J_\pm$ |j,m> is indeed an eigenfunction of J_z with eigenvalue $(m\pm1) \hbar$, $J_\pm$ |j,m> is not identical to |j,m±1>; it is only proportional to |j,m±1>:

$$J_\pm |j,m> = C^\pm_{j,m} |j,m\pm1>.$$

Explicit expressions for these $C^{\pm}_{j,m}$ coefficients will be obtained below. Notice also that because the $J_{\pm}$ |j,m>, and hence |j,m±1>, have the same J^2 eigenvalue as |j,m> (in fact, sequential application of $J_{\pm}$ can be used to show that all |j,m'>, for all m', have this same J^2 eigenvalue), the J^2 eigenvalue f(j,m) must be independent of m. For this reason, f can be labeled by one quantum number j.

iii. The J^2 Eigenvalues are Related to the Maximum and Minimum J_z Eigenvalues, Which are Related to One Another

Earlier, we showed that there exists a maximum and a minimum value for m, for any given total angular momentum. It is when one reaches these limiting cases that $J_{\pm}$ |j,m> = 0 applies. In particular,

$$J_+ \text{ |j,}m_{max}> = 0,$$

$$J_- \text{ |j,}m_{min}> = 0.$$

Applying the following identities:

$$J_- J_+ = J^2 - J_z{}^2 - \hbar J_z ,$$

$$J_+ J_- = J^2 - J_z{}^2 + \hbar J_z,$$

respectively, to |j,m_{max}> and |j,m_{min}> gives

$$\hbar^2 \{ f(j,m_{max}) - m_{max}{}^2 - m_{max} \} = 0,$$

$$\hbar^2 \{ f(j,m_{min}) - m_{min}{}^2 + m_{min} \} = 0,$$

which immediately gives the J^2 eigenvalue $f(j,m_{max})$ and $f(j,m_{min})$ in terms of m_{max} or m_{min}:

$$f(j,m_{max}) = m_{max}\,(m_{max}+1),$$

$$f(j,m_{min}) = m_{min}\,(m_{min}-1).$$

So, we now know the J^2 eigenvalues for $|j,m_{max}\rangle$ and $|j,m_{min}\rangle$. However, we earlier showed that $|j,m\rangle$ and $|j,m-1\rangle$ have the same J^2 eigenvalue (when we treated the effect of $J_\pm$ on $|j,m\rangle$) and that the J^2 eigenvalue is independent of m. If we therefore define the quantum number j to be m_{max} , we see that the J^2 eigenvalues are given by

$$J^2\,|j,m\rangle = \hbar^2\,j(j+1)\,|j,m\rangle.$$

We also see that

$$f(j,m) = j(j+1) = m_{max}\,(m_{max}+1) = m_{min}\,(m_{min}-1),$$

from which it follows that

$$m_{min} = -\,m_{max}\,.$$

iv. The j Quantum Number Can Be Integer or Half-Integer

The fact that the m-values run from j to -j in unit steps (because of the property of the $J_\pm$ operators), there clearly can be only integer or half-integer values for j. In the former case, the m quantum number runs over -j, -j+1, -j+2, ..., -j+(j-1), 0, 1, 2, ... j; in the latter, m runs over -j, -j+1, -j+2, ...-j+(j-1/2), 1/2, 3/2, ...j. Only integer and half-integer values can range from j to -j in steps of unity. Species whose intrinsic angular

momenta are integers are known as Bosons and those with half-integer spin are called Fermions.

v. More on $J_{\pm}$ |j,m>

Using the above results for the effect of $J_{\pm}$ acting on |j,m> and the fact that J_+ and J_- are adjoints of one another (two operators F and G are adjoints if $<\psi|F|\chi> = <G\psi|\chi>$, for all ψ and all χ) allows us to write:

$$<j,m| J_- J_+ |j,m> = <j,m| (J^2 - J_z^2 - \hbar J_z) |j,m>$$

$$= \hbar^2 \{j(j+1)-m(m+1)\} = <J_+<j,m| J_+|j,m> = (C^+_{j,m})^2,$$

where $C^+_{j,m}$ is the proportionality constant between $J_+|j,m>$ and the normalized function |j,m+1>. Likewise, the effect of J_- can be expressed as

$$<j,m| J_+ J_- |j,m> = <j,m| (J^2 - J_z^2 + \hbar J_z) |j,m>$$

$$= \hbar^2 \{j(j+1)-m(m-1)\} = <J_-<j,m| J_-|j,m> = (C^-_{j,m})^2,$$

where $C^-_{j,m}$ is the proportionality constant between J_- |j,m> and the normalized |j,m-1>. Thus, we can solve for $C^{\pm}_{j,m}$ after which the effect of $J_{\pm}$ on |j,m> is given by:

$$J_{\pm} |j,m> = \hbar \{j(j+1) - m(m\pm1)\}^{1/2} |j,m\pm1>.$$

2.7.3. Summary

The above results apply to any angular momentum operators. The essential findings can be summarized as follows:

(i) J^2 and J_z have complete sets of simultaneous eigenfunctions. We label these eigenfunctions |j,m>; they are orthonormal in both their m- and j-type indices: <j,m| j',m'> = $\delta_{m,m'} \delta_{j,j'}$.

(ii) These |j,m> eigenfunctions obey:

$$J^2 |j,m> = \hbar^2 j(j+1) |j,m>, \{ j= \text{integer or half-integer}\},$$

$$J_z |j,m> = \hbar m |j,m>, \{ m = -j, \text{ in steps of 1 to } +j\}.$$

(iii) The raising and lowering operators $J_\pm$ act on |j,m> to yield functions that are eigenfunctions of J^2 with the same eigenvalue as |j,m> and eigenfunctions of J_z with eigenvalue of $(m\pm1) \hbar$:

$$J_\pm |j,m> = \hbar \{j(j+1) - m(m\pm1)\}^{1/2} |j,m\pm1>.$$

(iv) When $J_\pm$ acts on the extremal states |j,j> or |j,-j>, respectively, the result is zero.

The results given above are, as stated, general. Any and all angular momenta have quantum mechanical operators that obey these equations. It is convention to designate specific kinds of angular momenta by specific letters; however, it should be kept in mind that no matter what letters are used, there are operators corresponding to J^2, J_z, and $J_\pm$ that obey relations as specified above, and there are eigenfunctions and eigenvalues that have all of the properties obtained above. For electronic or collisional orbital angular momenta, it is common to use L^2 and L_z ; for electron spin, S^2 and S_z are used; for nuclear spin I^2 and I_z are most common; and for molecular rotational angular momentum, N^2 and N_z are most common (although sometimes J^2 and J_z may be used). Whenever two or more angular momenta are combined or coupled to produce a total angular momentum, the latter is designated by J^2 and J_z.

2.7.4. Coupling of Angular Momenta

If the Hamiltonian under study contains terms that couple two or more angular momenta $\mathbf{J}(i)$, then only the components of the total angular momentum $\mathbf{J} = \Sigma_i \mathbf{J}(i)$ and the total $\mathbf{J}^2$ will commute with H. It is therefore essential to label the quantum states of the system by the eigenvalues of $\mathbf{J_z}$ and $\mathbf{J}^2$ and to construct variational trial or model wave functions that are eigenfunctions of these total angular momentum operators. The problem of angular momentum coupling has to do with how to combine eigenfunctions of the uncoupled angular momentum operators, which are given as simple products of the eigenfunctions of the individual angular momenta $\Pi_i |j_i,m_i\rangle$, to form eigenfunctions of J^2 and J_z.

a. Eigenfunctions of J_z

Because the individual elements of $\mathbf{J}$ are formed additively, but J^2 is not, it is straightforward to form eigenstates of

$$J_z = \Sigma_i J_z(i);$$

simple products of the form $\Pi_i |j_i,m_i\rangle$ are eigenfunctions of J_z:

$$J_z \, \Pi_i |j_i,m_i\rangle = \Sigma_k J_z(k) \, \Pi_i |j_i,m_i\rangle = \Sigma_k \hbar \, m_k \, \Pi_i |j_i,m_i\rangle,$$

and have J_z eigenvalues equal to the sum of the individual $m_k \hbar$ eigenvalues. Hence, to form an eigenfunction with specified J and M eigenvalues, one must combine only those product states $\Pi_i |j_i,m_i\rangle$ whose $m_i \hbar$ sum is equal to the specified M value.

b. Eigenfunctions of J^2; the Clebsch-Gordon Series

The task is then reduced to forming eigenfunctions $|J,M>$, given particular values for the $\{j_i\}$ quantum numbers. When coupling pairs of angular momenta $\{ |j,m>$ and $|j',m'>\}$, the total angular momentum states can be written, according to what we determined above, as

$$|J,M> = \Sigma_{m,m'} \; C^{J,M}_{j,m;j',m'} \; |j,m> \; |j',m'>,$$

where the coefficients $C^{J,M}_{j,m;j',m'}$ are called vector coupling coefficients (because angular momentum coupling is viewed much like adding two vectors **j** and **j'** to produce another vector **J**), and where the sum over m and m' is restricted to those terms for which m+m' = M. It is more common to express the vector coupling or so-called Clebsch-Gordon (CG) coefficients as $<j,m;j'm'|J,M>$ and to view them as elements of a matrix whose columns are labeled by the coupled-state J,M quantum numbers and whose rows are labeled by the quantum numbers characterizing the uncoupled product basis j,m;j',m'. It turns out that this matrix can be shown to be unitary so that the CG coefficients obey:

$$\Sigma_{m,m'} \; <j,m;j'm'|J,M>^* \; <j,m;j'm'|J',M'> = \delta_{J,J'} \; \delta_{M,M'}$$

and

$$\Sigma_{J,M} \quad <j,n;j'n'|J,M> \; <j,m;j'm'|J,M>^* \; = \delta_{n,m} \; \delta_{n',m'}.$$

This unitarity of the CG coefficient matrix allows the inverse of the relation giving coupled functions in terms of the product functions:

$$|J,M> = \Sigma_{m,m'} <j,m;j'm'|J,M> \; |j,m> \; |j',m'>$$

to be written as:

$$|j,m> |j',m'> = \Sigma_{J,M} <j,m;j'm'|J,M>* |J,M>$$

$$= \Sigma_{J,M} <J,M|j,m;j'm'> |J,M>.$$

This result expresses the product functions in terms of the coupled angular momentum functions.

c. Generation of the CG Coefficients

The CG coefficients can be generated in a systematic manner; however, they can also be looked up in books where they have been tabulated (e.g., see Table 2.4 of R. N. Zare, *Angular Momentum*, John Wiley, New York (1988)). Here, we will demonstrate the technique by which the CG coefficients can be obtained, but we will do so for rather limited cases and refer the reader to more extensive tabulations for more cases.

The strategy we take is to generate the |J,J> state (i.e., the state with maximum M-value) and to then use J_- to generate |J,J-1>, after which the state |J-1,J-1> (i.e., the state with one lower J-value) is constructed by finding a combination of the product states in terms of which |J,J-1> is expressed (because both |J,J-1> and |J-1,J-1> have the same M-value M=J-1) which is orthogonal to |J,J-1> (because |J-1,J-1> and |J,J-1> are eigenfunctions of the Hermitian operator J^2 corresponding to different eigenvalues, they must be orthogonal). This same process is then used to generate |J,J-2> |J-1,J-2> and (by orthogonality construction) |J-2,J-2>, and so on.

i. The States With Maximum and Minimum M-Values

We begin with the state |J,J> having the highest M-value. This state must be formed by taking the highest m and the highest m' values (i.e., m=j and m'=j'), and is given by:

$$|J,J> = |j,j> |j'j'>.$$

Only this one product is needed because only the one term with m=j and m'=j' contributes to the sum in the above CG series. The state

$$|J,-J> = |j,-j> |j',-j'>$$

with the minimum M-value is also given as a single product state.

Notice that these states have M-values given as ±(j+j'); since this is the maximum M-value, it must be that the J-value corresponding to this state is J= j+j'.

ii. States With One Lower M-Value But the Same J-Value

Applying J_- to $|J,J>$, and expressing J_- as the sum of lowering operators for the two individual angular momenta:

$$J_- = J_-(1) + J_-(2)$$

gives

$$J_-|J,J> = \hbar\{J(J+1) -J(J-1)\}^{1/2} |J,J-1>$$

$$= (J_-(1) + J_-(2)) |j,j> |j'j'>$$

$$= \hbar\{j(j+1) - j(j-1)\}^{1/2} |j,j-1> |j',j'> + \hbar\{j'(j'+1)-j'(j'-1)\}^{1/2} |j,j> |j',j'-1>.$$

This result expresses $|J,J-1>$ as follows:

$$|J,J-1>= [\{j(j+1)-j(j-1)\}^{1/2} |j,j-1> |j',j'>$$

$$+ \{j'(j'+1)-j'(j'-1)\}^{1/2} |j,j> |j',j'-1>] \{J(J+1) -J(J-1)\}^{-1/2};$$

that is, the |J,J-1> state, which has M=J-1, is formed from the two product states |j,j-1> |j',j'> and |j,j> |j',j'-1> that have this same M-value.

iii. States With One Lower J-Value

To find the state |J-1,J-1> that has the same M-value as the one found above but one lower J-value, we must construct another combination of the two product states with M=J-1 (i.e., |j,j-1> |j',j'> and |j,j> |j',j'-1>) that is orthogonal to the combination representing |J,J-1>; after doing so, we must scale the resulting function so it is properly normalized. In this case, the desired function is:

$$|J-1,J-1> = [\{j(j+1)-j(j-1)\}^{1/2} |j,j> |j',j'-1>$$

$$- \{j'(j'+1)-j'(j'-1)\}^{1/2} |j,j-1> |j',j'>] \{J(J+1)-J(J-1)\}^{-1/2} .$$

It is straightforward to show that this function is indeed orthogonal to |J,J-1>.

iv. States With Even One Lower J-Value

Having expressed |J,J-1> and |J-1,J-1> in terms of |j,j-1> |j',j'> and |j,j> |j',j'-1>, we are now prepared to carry on with this stepwise process to generate the states |J,J-2>, |J-1,J-2> and |J-2,J-2> as combinations of the product states with M=J-2. These product states are |j,j-2> |j',j'>, |j,j> |j',j'-2>, and |j,j-1> |j',j'-1>. Notice that there are precisely as many product states whose m+m' values add up to the desired M-value as there are total angular momentum states that must be constructed (there are three of each in this case).

The steps needed to find the state |J-2,J-2> are analogous to those taken above:
a. One first applies J_ to |J-1,J-1> and to |J,J-1> to obtain |J-1,J-2> and |J,J-2>, respectively as combinations of |j,j-2> |j',j'>, |j,j> |j',j'-2>, and |j,j-1> |j',j'-1>.
b. One then constructs |J-2,J-2> as a linear combination of the |j,j-2> |j',j'>, |j,j> |j',j'-2>, and |j,j-1> |j',j'-1> that is orthogonal to the combinations found for |J-1,J-2> and |J,J-2>.

Once |J-2,J-2> is obtained, it is then possible to move on to form |J,J-3>, |J-1,J-3>, and |J-2,J-3> by applying J_ to the three states obtained in the preceding application of the process, and to then form |J-3,J-3> as the combination of |j,j-3> |j',j'>, |j,j> |j',j'-3>,

|j,j-2> |j',j'-1>, |j,j-1> |j',j'-2> that is orthogonal to the combinations obtained for |J,J-3>, |J-1,J-3>, and |J-2,J-3>.

Again notice that there are precisely the correct number of product states (four here) as there are total angular momentum states to be formed. In fact, the product states and the total angular momentum states are equal in number and are both members of orthonormal function sets (because $J^2(1)$, $J_z(1)$, $J^2(2)$, and $J_z(2)$ as well as J^2 and J_z are Hermitian operators which have complete sets of orthonormal eigenfunctions). This is why the CG coefficient matrix is unitary; because it maps one set of orthonormal functions to another, with both sets containing the same number of functions.

d. An Example

Let us consider an example in which the spin and orbital angular momenta of the Si atom in its ^3P ground state can be coupled to produce various ^3P_J states. In this case, the specific values for j and j' are j=S=1 and j'=L=1. We could, of course take j=L=1 and j'=S=1, but the final wave functions obtained would span the same space as those we are about to determine.

The state with highest M-value is the $^3P(M_s=1, M_L=1)$ state, which can be represented by the product of an $\alpha\alpha$ spin function (representing S=1, $M_s=1$) and a $3p_13p_0$ spatial function (representing L=1, $M_L=1$), where the first function corresponds to the first open-shell orbital and the second function to the second open-shell orbital. Thus, the maximum M-value is M= 2 and corresponds to a state with J=2:

$$|J=2,M=2> = |2,2> = \alpha\alpha\ 3p_13p_0 .$$

Clearly, the state |2,-2> would be given as $\beta\beta\ 3p_{-1}3p_0$.

The states |2,1> and |1,1> with one lower M-value are obtained by applying $J_- = S_- + L_-$ to |2,2> as follows:

$$J_-\ |2,2> = \hbar\{J(J+1)-M(M-1)\}^{1/2}\ |2,1> = \hbar\{2(3)-2(1)\}^{1/2}\ |2,1>$$

$$= (S_- + L_-)\ \alpha\alpha\ 3p_13p_0 \ .$$

To apply S_- or L_- to $\alpha\alpha$ $3p_13p_0$, one must realize that each of these operators is, in turn, a sum of lowering operators for each of the two open-shell electrons:

$$S_- = S_-(1) + S_-(2),$$

$$L_- = L_-(1) + L_-(2).$$

The result above can therefore be continued as

$$(S_- + L_-)\ \alpha\alpha\ 3p_13p_0 = \hbar\{1/2(3/2)\text{-}1/2(\text{-}1/2)\}^{1/2}\ \beta\alpha\ 3p_13p_0$$

$$+\ \hbar\{1/2(3/2)\text{-}1/2(\text{-}1/2)\}^{1/2}\ \alpha\beta\ 3p_13p_0$$

$$+\ \hbar\{1(2)\text{-}1(0)\}^{1/2}\ \alpha\alpha\ 3p_03p_0$$

$$+\ \hbar\{1(2)\text{-}0(\text{-}1)\}^{1/2}\ \alpha\alpha\ 3p_13p_{-1}.$$

So, the function $|2,1\rangle$ is given by

$$|2,1\rangle = [\beta\alpha\ 3p_13p_0 + \alpha\beta\ 3p_13p_0 + \{2\}^{1/2}\ \alpha\alpha\ 3p_03p_0$$

$$+\ \{2\}^{1/2}\ \alpha\alpha\ 3p_13p_{-1}]/2,$$

which can be rewritten as:

$$|2,1\rangle = [(\beta\alpha + \alpha\beta)3p_13p_0 + \{2\}^{1/2}\ \alpha\alpha\ (3p_03p_0 + 3p_13p_{-1})]/2.$$

Writing the result in this way makes it clear that $|2,1\rangle$ is a combination of the product states $|S=1,M_S=0\rangle$ $|L=1,M_L=1\rangle$ (the terms containing $|S=1,M_S=0\rangle = 2^{-1/2}(\alpha\beta+\beta\alpha)$) and $|S=1,M_S=1\rangle$ $|L=1,M_L=0\rangle$ (the terms containing $|S=1,M_S=1\rangle = \alpha\alpha$).

There is a good chance that some readers have noticed that some of the terms in the $|2,1\rangle$ function would violate the Pauli exclusion principle. In particular, the term $\alpha\alpha$ $3p_0 3p_0$ places two electrons into the same orbitals and with the same spin. Indeed, this electronic function would indeed violate the Pauli principle, and it should not be allowed to contribute to the final Si ^3P_J wave functions we are trying to form. The full resolution of how to deal with this paradox is given in the following Subsection, but for now let me say the following:

(i) Once you have learned that all of the spin-orbital product functions shown for $|2,1\rangle$ (e.g., $\alpha\alpha$ $3p_0 3p_0$, $(\beta\alpha + \alpha\beta)3p_1 3p_0$, and $\alpha\alpha$ $3p_1 3p_{-1}$) represent Slater determinants (we deal with this in the next Subsection) that are antisymmetric with respect to permutation of any pair of electrons, you will understand that the Slater determinant corresponding to $\alpha\alpha$ $3p_0 3p_0$ vanishes.

(ii) If, instead of considering the $3s^2 3p^2$ configuration of Si, we wanted to generate wave functions for the $3s^2 3p^1 4p^1$ ^3P_J states of Si, the same analysis as shown above would pertain, except that now the $|2,1\rangle$ state would have a contribution from $\alpha\alpha$ $3p_0 4p_0$. This contribution does not violate the Pauli principle, and its Slater determinant does not vanish.

So, for the remainder of this treatment of the ^3P_J states of Si, don't worry about terms arising that violate the Pauli principle; they will not contribute because their Slater determinants will vanish.

To form the other function with M=1, the $|1,1\rangle$ state, we must find another combination of $|S=1,M_S=0\rangle$ $|L=1,M_L=1\rangle$ and $|S=1,M_S=1\rangle$ $|L=1,M_L=0\rangle$ that is orthogonal to $|2,1\rangle$ and is normalized. Since

$$|2,1\rangle = 2^{-1/2} [|S=1,M_S=0\rangle |L=1,M_L=1\rangle + |S=1,M_S=1\rangle |L=1,M_L=0\rangle],$$

we immediately see that the requisite function is

$$|1,1\rangle = 2^{-1/2} [|S=1,M_S=0\rangle |L=1,M_L=1\rangle - |S=1,M_S=1\rangle |L=1,M_L=0\rangle].$$

In the spin-orbital notation used above, this state is:

$$|1,1\rangle = [(\beta\alpha + \alpha\beta)3p_1 3p_0 - \{2\}^{1/2} \alpha\alpha (3p_0 3p_0 + 3p_1 3p_{-1})]/2.$$

Thus far, we have found the ^3P_J states with J=2, M=2; J=2, M=1; and J=1, M=1.

To find the ^3P_J states with J=2, M=0; J=1, M=0; and J=0, M=0, we must once again apply the J_- tool. In particular, we apply J_- to $|2,1\rangle$ to obtain $|2,0\rangle$ and we apply J_- to $|1,1\rangle$ to obtain $|1,0\rangle$, each of which will be expressed in terms of $|S=1,M_S=0\rangle$ $|L=1,M_L=0\rangle$, $|S=1,M_S=1\rangle |L=1,M_L=-1\rangle$, and $|S=1,M_S=-1\rangle |L=1,M_L=1\rangle$. The $|0,0\rangle$ state is then constructed to be a combination of these same product states which is orthogonal to $|2,0\rangle$ and to $|1,0\rangle$. The results are as follows:

$$|J=2,M=0\rangle = 6^{-1/2}[2 |1,0\rangle |1,0\rangle + |1,1\rangle |1,-1\rangle + |1,-1\rangle |1,1\rangle],$$

$$|J=1,M=0\rangle = 2^{-1/2}[|1,1\rangle |1,-1\rangle - |1,-1\rangle |1,1\rangle],$$

$$|J=0, M=0\rangle = 3^{-1/2}[|1,0\rangle |1,0\rangle - |1,1\rangle |1,-1\rangle - |1,-1\rangle |1,1\rangle],$$

where, in all cases, a short hand notation has been used in which the $|S,M_S\rangle |L,M_L\rangle$ product stated have been represented by their quantum numbers with the spin function always appearing first in the product. To finally express all three of these new functions in terms of spin-orbital products it is necessary to give the $|S,M_S\rangle |L,M_L\rangle$ products with M=0 in terms of these products. For the spin functions, we have:

$$|S=1,M_S=1\rangle = \alpha\alpha,$$

$$|S=1,M_S=0\rangle = 2^{-1/2}(\alpha\beta+\beta\alpha).$$

$$|S=1, M_S=-1\rangle = \beta\beta.$$

For the orbital product function, we have:

$$|L=1, M_L=1\rangle = 3p_1 3p_0 ,$$

$$|L=1, M_L=0\rangle = 2^{-1/2}(3p_0 3p_0 + 3p_1 3p_{-1}),$$

$$|L=1, M_L=-1\rangle = 3p_0 3p_{-1}.$$

e. Coupling Angular Momenta of Equivalent Electrons

If equivalent angular momenta are coupled (e.g., to couple the orbital angular momenta of a p^2 or d^3 configuration), there is a tool one can use to determine which of the term symbols violate the Pauli principle. To carry out this step, one forms all possible unique (determinental) product states with non-negative M_L and M_S values and arranges them into groups according to their M_L and M_S values. For example, the "boxes" appropriate to the p^2 orbital occupancy that we considered earlier for Si are shown below:

M_L	2	1	0
M_S 1		$|p_1\alpha p_0\alpha|$	$|p_1\alpha p_{-1}\alpha|$
0	$|p_1\alpha p_1\beta|$	$|p_1\alpha p_0\beta|, |p_0\alpha p_1\beta|$	$|p_1\alpha p_{-1}\beta|,$ $|p_{-1}\alpha p_1\beta|,$ $|p_0\alpha p_0\beta|$

There is no need to form the corresponding states with negative M_L or negative M_S values because they are simply "mirror images" of those listed above. For example, the state with $M_L = -1$ and $M_S = -1$ is $|p_{-1}\beta p_0\beta|$, which can be obtained from the $M_L = 1$, M_S

= 1 state $|p_1\alpha p_0\alpha|$ by replacing α by β and replacing p_1 by p_{-1}.

Given the box entries, one can identify those term symbols that arise by applying the following procedure over and over until all entries have been accounted for:

i. One identifies the highest M_S value (this gives a value of the total spin quantum number that arises, S) in the box. For the above example, the answer is S = 1.

ii. For all product states of <u>this</u> M_S value, one identifies the highest M_L value (this gives a value of the total orbital angular momentum, L, that can arise <u>for this S</u>). For the above example, the highest M_L within the M_S =1 states is M_L = 1 (not M_L = 2), hence L=1.

iii. Knowing an S, L combination, one knows the first term symbol that arises from this configuration. In the p^2 example, this is ^3P.

iv. Because the level with this L and S quantum numbers contains (2L+1)(2S+1) states with M_L and M_S quantum numbers running from -L to L and from -S to S, respectively, one must remove from the original box this number of product states. To do so, one simply erases from the box one entry with each such M_L and M_S value. Actually, since the box need only show those entries with non-negative M_L and M_S values, only these entries need be explicitly deleted. In the ^3P example, this amounts to deleting nine product states with M_L, M_S values of 1,1; 1,0; 1,-1; 0,1; 0,0; 0,-1; -1,1; -1,0; -1,-1.

v. After deleting these entries, one returns to step 1 and carries out the process again. For the p^2 example, the box after deleting the first nine product states looks as follows (those that appear in italics should be viewed as already deleted in counting all of the ^3P states):

M_L	2	1	0
M_S 1		*$|p_1\alpha p_0\alpha|$*	*$|p_1\alpha p_{-1}\alpha|$*
0	$|p_1\alpha p_1\beta|$	*$|p_1\alpha p_0\beta|$, $|p_0\alpha p_1\beta|$*	*$|p_1\alpha p_{-1}\beta|$,*
			$|p_{-1}\alpha p_1\beta|$,
			$|p_0\alpha p_0\beta|$

It should be emphasized that the process of deleting or crossing off entries in various M_L,

M_S boxes involves only counting how many states there are; by no means do we identify the particular L,S,M_L,M_S wave functions when we cross out any particular entry in a box. For example, when the $|p_1\alpha p_0\beta|$ product is deleted from the $M_L = 1$, $M_S = 0$ box in accounting for the states in the ^3P level, we do not claim that $|p_1\alpha p_0\beta|$ itself is a member of the ^3P level; the $|p_0\alpha p_1\beta|$ product state could just as well been eliminated when accounting for the ^3P states.

Returning to the p^2 example at hand, after the ^3P term symbol's states have been accounted for, the highest M_S value is 0 (hence there is an S=0 state), and within this M_S value, the highest M_L value is 2 (hence there is an L=2 state). This means there is a ^1D level with five states having M_L = 2,1,0,-1,-2. Deleting five appropriate entries from the above box (again denoting deletions by italics) leaves the following box:

M_L	2	1	0
M_S 1		$|p_1\alpha p_0\alpha|$	$|p_1\alpha p_{-1}\alpha|$
0	$|p_1\alpha p_1\beta|$	$|p_1\alpha p_0\beta|$, $|p_0\alpha p_1\beta|$	$|p_1\alpha p_{-1}\beta|$, $|p_{-1}\alpha p_1\beta|$, $|p_0\alpha p_0\beta|$

The only remaining entry, which thus has the highest M_S and M_L values, has $M_S = 0$ and $M_L = 0$. Thus there is also a ^1S level in the p^2 configuration.

Thus, unlike the non-equivalent $3p^1 4p^1$ case, in which ^3P, ^1P, ^3D, ^1D, ^3S, and ^1S levels arise, only the ^3P, ^1D, and ^1S arise in the p^2 situation. This "box method" is useful to carry out whenever one is dealing with equivalent angular momenta.

If one has mixed equivalent and non-equivalent angular momenta, one can determine all possible couplings of the equivalent angular momenta using this method and then use the simpler vector coupling method to add the non-equivalent angular

momenta to <u>each</u> of these coupled angular momenta. For example, the p^2d^1 configuration can be handled by vector coupling (using the straightforward non-equivalent procedure) L=2 (the d orbital) and S=1/2 (the third electron's spin) to <u>each</u> of ^3P, ^1D, and ^1S arising from the p^2 configuration. The result is ^4F, ^4D, ^4P, ^2F, ^2D, ^2P, ^2G, ^2F, ^2D, ^2P, ^2S, and ^2D.

2.8. Rotations of Molecules

2.8.1. Rotational Motion For Rigid Diatomic and Linear Polyatomic Molecules

This Schrödinger equation relates to the rotation of diatomic and linear polyatomic molecules. It also arises when treating the angular motions of electrons in any spherically symmetric potential.

A diatomic molecule with fixed bond length R rotating in the absence of any external potential is described by the following Schrödinger equation:

$$- \hbar^2/2\mu \; \{(R^2\sin\theta)^{-1}\partial/\partial\theta \; (\sin\theta \; \partial/\partial\theta) + (R^2\sin^2\theta)^{-1} \; \partial^2/\partial\phi^2 \} \; \psi \; = E \; \psi$$

or

$$L^2\psi/2\mu R^2 = E \; \psi,$$

where L^2 is the square of the total angular momentum operator $L_x^2 + L_y^2 + L_z^2$ expressed in polar coordinates above. The angles θ and ϕ describe the orientation of the diatomic molecule's axis relative to a laboratory-fixed coordinate system, and μ is the reduced mass of the diatomic molecule $\mu=m_1m_2/(m_1+m_2)$. The differential operators can be seen to be exactly the same as those that arose in the hydrogen-like-atom case discussed earlier in this Chapter. Therefore, the same spherical harmonics that served as the angular parts of the wave function in the hydrogen-atom case now serve as the entire wave function for the so-called rigid rotor: $\psi = Y_{J,M}(\theta,\phi)$. These are exactly the same functions as we

plotted earlier when we graphed the s (L=0), p (L=1), and d (L=2) orbitals. The energy eigenvalues corresponding to each such eigenfunction are given as:

$$E_J = \hbar^2 \, J(J+1)/(2\mu R^2) = B \, J(J+1)$$

and are independent of M. Thus each energy level is labeled by J and is 2J+1-fold degenerate (because M ranges from -J to J). Again, this is just like we saw when we looked at the hydrogen orbitals; the p orbitals are 3-fold degenerate and the d orbitals are 5-fold degenerate. The so-called rotational constant B (defined as $\hbar^2/2\mu R^2$) depends on the molecule's bond length and reduced mass. Spacings between successive rotational levels (which are of spectroscopic relevance because, as shown in Chapter 6, angular momentum selection rules often restrict the changes ΔJ in J that can occur upon photon absorption to 1,0, and -1) are given by

$$\Delta E = B \, (J+1)(J+2) - B \, J(J+1) = 2B(J+1).$$

These energy spacings are of relevance to microwave spectroscopy which probes the rotational energy levels of molecules. In fact, microwave spectroscopy offers the most direct way to determine molecular rotational constants and hence molecular bond lengths.

   The rigid rotor provides the most commonly employed approximation to the rotational energies and wave functions of linear molecules. As presented above, the model restricts the bond length to be fixed. Vibrational motion of the molecule gives rise to changes in R, which are then reflected in changes in the rotational energy levels (i.e., there are different B values for different vibrational levels). The coupling between rotational and vibrational motion gives rise to rotational B constants that depend on vibrational state as well as dynamical couplings, called centrifugal distortions, which cause the total ro-vibrational energy of the molecule to depend on rotational and vibrational quantum numbers in a non-separable manner.

   Within this rigid rotor model, the absorption spectrum of a rigid diatomic molecule should display a series of peaks, each of which corresponds to a specific J → J + 1 transition. The energies at which these peaks occur should grow linearly with J as

shown above. An example of such a progression of rotational lines is shown in the Fig. 2.23.
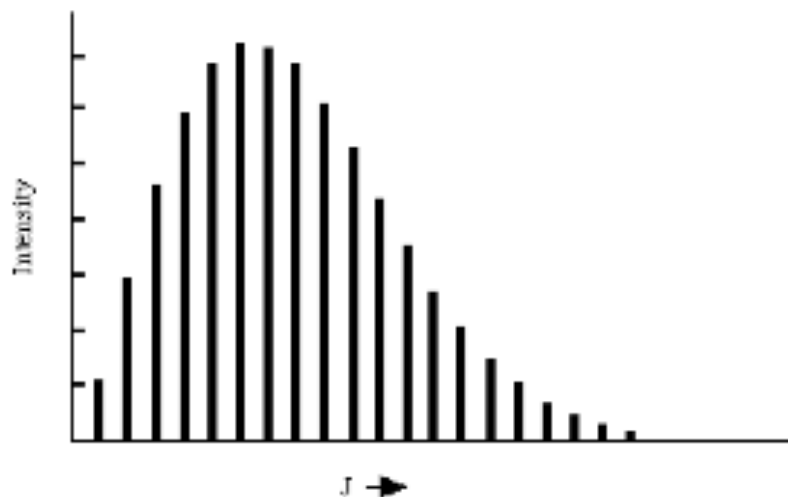

Figure 2.23. Typical rotational absorption profile showing intensity vs. J value of the absorbing level

The energies at which the rotational transitions occur appear to fit the $\Delta E = 2B\,(J+1)$ formula rather well. The intensities of transitions from level J to level J+1 vary strongly with J primarily because the population of molecules in the absorbing level varies with J. These populations P_J are given, when the system is at equilibrium at temperature T, in terms of the degeneracy (2J+1) of the Jth level and the energy of this level B J(J+1) by the Boltzmann formula:

$$P_J = Q^{-1}\,(2J+1)\,\exp(-BJ(J+1)/kT),$$

where Q is the rotational partition function:

$$Q = \Sigma_J\,(2J+1)\,\exp(-BJ(J+1)/kT).$$

For low values of J, the degeneracy is low and the exp(-BJ(J+1)/kT) factor is near unity. As J increases, the degeneracy grows linearly but the exp(-BJ(J+1)/kT) factor decreases

more rapidly. As a result, there is a value of J, given by taking the derivative of (2J+1) exp(-BJ(J+1)/kT) with respect to J and setting it equal to zero,

$$2J_{max} + 1 = \sqrt{2kT/B}$$

at which the intensity of the rotational transition is expected to reach its maximum. This behavior is clearly displayed in the above figure.

The eigenfunctions belonging to these energy levels are the spherical harmonics $Y_{L,M}(\theta,\phi)$ which are normalized according to

$$\int_0^\pi \int_0^{2\pi} (Y^*_{L,M}(\theta,\phi)Y_{L',M'}(\theta,\phi)\sin\theta d\phi d\theta = \delta_{L,L'}\delta_{M,M'} .$$

As noted above, these functions are identical to those that appear in the solution of the angular part of Hydrogenic atoms. The above energy levels and eigenfunctions also apply to the rotation of rigid linear polyatomic molecules; the only difference is that the moment of inertia I entering into the rotational energy expression, which is μR^2 for a diatomic, is given by

$$I = \Sigma_a m_a R_a^2$$

where m_a is the mass of the ath atom and R_a is its distance from the center of mass of the molecule to this atom.

2.8.2. Rotational Motions of Rigid Non-Linear Molecules

a. The Rotational Kinetic Energy

The classical rotational kinetic energy for a rigid polyatomic molecule is

$$H_{rot} = J_a^2/2I_a + J_b^2/2I_b + J_c^2/2I_c$$

where the I_k (k = a, b, c) are the three principal moments of inertia of the molecule (the eigenvalues of the moment of inertia tensor). This tensor has elements in a Cartesian coordinate system (K, K' = X, Y, Z), whose origin is located at the center of mass of the molecule, that can be computed as:

$$I_{K,K} = \Sigma_j \, m_j \, (R_j{}^2 - R^2{}_{K,j}) \qquad \text{(for K = K')}$$

$$I_{K,K'} = - \Sigma_j \, m_j \, R_{K,j} \, R_{K',j} \qquad \text{(for K} \neq \text{K')}.$$

As discussed in more detail in R. N. Zare, *Angular Momentum*, John Wiley, New York (1988), the components of the corresponding quantum mechanical angular momentum operators along the three principal axes are:

$$J_a = -i\hbar \, \cos\chi \, [\cot\theta \, \partial/\partial\chi - (\sin\theta)^{-1}\partial/\partial\phi \,] - i\hbar \, \sin\chi \, \partial/\partial\theta$$

$$J_b = i\hbar \, \sin\chi \, [\cot\theta \, \partial/\partial\chi - (\sin\theta)^{-1}\partial/\partial\phi \,] - i\hbar \, \cos\chi \, \partial/\partial\theta$$

$$J_c = - \, i\hbar \, \partial/\partial\chi.$$

The angles θ, ϕ, and χ are the Euler angles needed to specify the orientation of the rigid molecule relative to a laboratory-fixed coordinate system. The corresponding square of the total angular momentum operator J^2 can be obtained as

$$J^2 = J_a{}^2 + J_b{}^2 + J_c{}^2$$

$$= - \hbar^2 \, \partial^2/\partial\theta^2 - \hbar^2\cot\theta \, \partial/\partial\theta$$

$$+ \hbar^2 \, (1/\sin^2\theta) \, (\partial^2/\partial\phi^2 + \partial^2/\partial\chi^2 - 2 \cos\theta\partial^2/\partial\phi\partial\chi),$$

and the component along the lab-fixed Z axis J_Z is $- i\hbar\, \partial/\partial\phi$ as we saw much earlier in this text.

b. The Eigenfunctions and Eigenvalues for Special Cases
i. Spherical Tops

When the three principal moment of inertia values are identical, the molecule is termed a spherical top. In this case, the total rotational energy can be expressed in terms of the total angular momentum operator J^2

$$H_{rot} = J^2/2I.$$

As a result, the eigenfunctions of H_{rot} are those of J^2 and J_a as well as J_Z both of which commute with J^2 and with one another. J_Z is the component of **J** along the lab-fixed Z-axis and commutes with J_a because $J_Z = - i\hbar\, \partial/\partial\phi$ and $J_a = - i\hbar\, \partial/\partial\chi$ act on different angles. The energies associated with such eigenfunctions are

$$E(J,K,M) = \hbar^2\, J(J+1)/2I^2,$$

for all K (i.e., J_a quantum numbers) ranging from -J to J in unit steps and for all M (i.e., J_Z quantum numbers) ranging from -J to J. Each energy level is therefore $(2J + 1)^2$ degenerate because there are $2J + 1$ possible K values and $2J + 1$ possible M values for each J.

The eigenfunctions $|J,M,K\rangle$ of J^2, J_Z and J_a , are given in terms of the set of so-called rotation matrices $D_{J,M,K}$:

$$|J,M,K\rangle = \sqrt{\frac{2J + 1}{8\,\pi^2}}\ D^*_{J,M,K}(\theta,\phi,\chi)$$

which obey

$$J^2 |J,M,K\rangle = \hbar^2 \, J(J+1) \, |J,M,K\rangle,$$

$$J_a \, |J,M,K\rangle = \hbar \, K \, |J,M,K\rangle,$$

$$J_Z \, |J,M,K\rangle = \hbar \, M \, |J,M,K\rangle.$$

These $D_{J,M,K}$ functions are proportional to the spherical harmonics $Y_{J,M}(\theta,\phi)$ multiplied by $\exp(iK\chi)$, which reflects its χ-dependence.

ii. Symmetric Tops

Molecules for which two of the three principal moments of inertia are equal are called symmetric tops. Those for which the unique moment of inertia is smaller than the other two are termed prolate symmetric tops; if the unique moment of inertia is larger than the others, the molecule is an oblate symmetric top. An American football is prolate, and a Frisbee is oblate.

Again, the rotational kinetic energy, which is the full rotational Hamiltonian, can be written in terms of the total rotational angular momentum operator J^2 and the component of angular momentum along the axis with the unique principal moment of inertia:

$$H_{rot} = J^2/2I + J_a^2\{1/2I_a - 1/2I\}, \text{ for prolate tops}$$

$$H_{rot} = J^2/2I + J_c^2\{1/2I_c - 1/2I\}, \text{ for oblate tops.}$$

Here, the moment of inertia I denotes that moment that is common to two directions; that is, I is the non-unique moment of inertia. As a result, the eigenfunctions of H_{rot} are those of J^2 and J_a or J_c (and of J_Z), and the corresponding energy levels are:

$$E(J,K,M) = \hbar^2 \, J(J+1)/2I^2 + \hbar^2 \, K^2 \, \{1/2I_a - 1/2I\},$$

for prolate tops

$$E(J,K,M) = \hbar^2 \, J(J+1)/2I^2 + \hbar^2 \, K^2 \, \{1/2I_c - 1/2I\},$$

for oblate tops, again for K and M (i.e., J_a or J_c and J_Z quantum numbers, respectively) ranging from -J to J in unit steps. Since the energy now depends on K, these levels are only 2J + 1 degenerate due to the 2J + 1 different M values that arise for each J value. Notice that for prolate tops, because I_a is smaller than I, the energies increase with increasing K for given J. In contrast, for oblate tops, since I_c is larger than I, the energies decrease with K for given J. The eigenfunctions |J, M,K> are the same rotation matrix functions as arise for the spherical-top case, so they do not require any further discussion at this time.

iii. Asymmetric Tops

The rotational eigenfunctions and energy levels of a molecule for which all three principal moments of inertia are distinct (a so-called asymmetric top) cannot analytically be expressed in terms of the angular momentum eigenstates and the J, M, and K quantum numbers. In fact, no one has ever solved the corresponding Schrödinger equation for this case. However, given the three principal moments of inertia I_a, I_b, and I_c, a matrix representation of each of the three contributions to the rotational Hamiltonian

$$H_{rot} = J_a{}^2/2I_a + J_b{}^2/2I_b + J_c{}^2/2I_c$$

can be formed within a basis set of the {|J, M, K>} rotation-matrix functions discussed earlier. This matrix will not be diagonal because the |J, M, K> functions are not eigenfunctions of the asymmetric top H_{rot}. However, the matrix can be formed in this basis and subsequently brought to diagonal form by finding its eigenvectors $\{C_{n, J,M,K}\}$ and its eigenvalues $\{E_n\}$. The vector coefficients express the asymmetric top eigenstates as

$$\psi_n(\theta, \phi, \chi) = \Sigma_{J, M, K} C_{n, J, M, K} |J, M, K\rangle.$$

Because the total angular momentum J^2 still commutes with H_{rot}, each such eigenstate will contain only one J-value, and hence ψ_n can also be labeled by a J quantum number:

$$\psi_{n, J}(\theta, \phi, \chi) = \Sigma_{M, K} C_{n, J, M, K} |J, M, K\rangle.$$

To form the only non-zero matrix elements of H_{rot} within the $|J, M, K\rangle$ basis, one can use the following properties of the rotation-matrix functions (see, for example, R. N. Zare, *Angular Momentum*, John Wiley, New York (1988)):

$$\langle J, M, K| J_a{}^2 | J, M, K\rangle = \langle J, M, K| J_b{}^2 | J, M, K\rangle$$

$$= 1/2 \langle J, M, K| J^2 - J_c{}^2 | J, M, K\rangle = \hbar^2 [J(J+1) - K^2],$$

$$\langle J, M, K| J_c{}^2 | J, M, K\rangle = \hbar^2 K^2,$$

$$\langle J, M, K| J_a{}^2 | J, M, K \pm 2\rangle = - \langle J, M, K| J_b{}^2 | J, M, K \pm 2\rangle$$

$$= \hbar^2 [J(J+1) - K(K \pm 1)]^{1/2} [J(J+1) - (K \pm 1)(K \pm 2)]^{1/2}$$

$$\langle J, M, K| J_c{}^2 | J, M, K \pm 2\rangle = 0.$$

Each of the elements of $J_c{}^2$, $J_a{}^2$, and $J_b{}^2$ must, of course, be multiplied, respectively, by $1/2I_c$, $1/2I_a$, and $1/2I_b$ and summed together to form the matrix representation of H_{rot}. The diagonalization of this matrix then provides the asymmetric top energies and wave functions.

2.9. Vibrations of Molecules

This Schrödinger equation forms the basis for our thinking about bond stretching and angle bending vibrations as well as collective vibrations in solids called phonons.

The radial motion of a diatomic molecule in its lowest (J=0) rotational level can be described by the following Schrödinger equation:

$$- (\hbar^2/2\mu) \, r^{-2} \partial/\partial r \, (r^2 \partial/\partial r) \, \psi + V(r) \, \psi = E \, \psi,$$

where μ is the reduced mass $\mu = m_1 m_2/(m_1+m_2)$ of the two atoms. If the molecule is rotating, then the above Schrödinger equation has an additional term $J(J+1) \, \hbar^2/2\mu \, r^{-2} \, \psi$ on its left-hand side. Thus, each rotational state (labeled by the rotational quantum number J) has its own vibrational Schrödinger equation and thus its own set of vibrational energy levels and wave functions. It is common to examine the J=0 vibrational problem and then to use the vibrational levels of this state as approximations to the vibrational levels of states with non-zero J values (treating the vibration-rotation coupling via perturbation theory). Let us thus focus on the J=0 situation.

By substituting $\psi = F(r)/r$ into this equation, one obtains an equation for F(r) in which the differential operators appear to be less complicated:

$$- \hbar^2/2\mu \, d^2F/dr^2 + V(r) \, F = E \, F.$$

This equation is exactly the same as the equation seen earlier in this text for the radial motion of the electron in the hydrogen-like atoms except that the reduced mass μ replaces the electron mass m and the potential V(r) is not the Coulomb potential.

If the vibrational potential is approximated as a quadratic function of the bond displacement $x = r - r_e$ expanded about the equilibrium bond length r_e where V has its minimum:

$$V = 1/2 \ k(r-r_e)^2,$$

the resulting harmonic-oscillator equation can be solved exactly. Because the potential V grows without bound as x approaches ∞ or $-\infty$, only bound-state solutions exist for this model problem. That is, the motion is confined by the nature of the potential, so no continuum states exist in which the two atoms bound together by the potential are dissociated into two separate atoms.

In solving the radial differential equation for this potential, the large-r behavior is first examined. For large-r, the equation reads:

$$d^2F/dx^2 = 1/2 \ k \ x^2 \ (2\mu/\hbar^2) \ F = (k\mu/\hbar^2) \ x^2 \ F,$$

where $x = r-r_e$ is the bond displacement away from equilibrium. Defining $\beta^2 = (k\mu/\hbar^2)$ and $\xi = \beta^{1/2} x$ as a new scaled radial coordinate, and realizing that

$$d^2/dx^2 = \beta \ d^2/d\xi^2$$

allows the large-r Schrödinger equation to be written as:

$$d^2F/d\xi^2 = \xi^2 F$$

which has the solution

$$F_{large-r} = \exp(- \xi^2/2).$$

The general solution to the radial equation is then expressed as this large-r solution multiplied by a power series in the ζ variable:

$$F = \exp(- \xi^2/2) \sum_{n=0} \xi^n C_n ,$$

where the C_n are coefficients to be determined. Substituting this expression into the full radial equation generates a set of recursion equations for the C_n amplitudes. As in the solution of the hydrogen-like radial equation, the series described by these coefficients is divergent unless the energy E happens to equal specific values. It is this requirement that the wave function not diverge so it can be normalized that yields energy quantization. The energies of the states that arise by imposing this non-divergence condition are given by:

$$E_n = \hbar \, (k/\mu)^{1/2} \, (n+1/2),$$

and the eigenfunctions are given in terms of the so-called Hermite polynomials $H_n(y)$ as follows:

$$\psi_n(x) = (n! \, 2^n)^{-1/2} \, (\beta/\pi)^{1/4} \exp(-\beta x^2/2) \, H_n(\beta^{1/2} \, x),$$

where $\beta = (k\mu/\hbar^2)^{1/2}$. Within this harmonic approximation to the potential, the vibrational energy levels are evenly spaced:

$$\Delta E = E_{n+1} - E_n = \hbar \, (k/\mu)^{1/2} \, .$$

In experimental data such evenly spaced energy level patterns are seldom seen; most commonly, one finds spacings $E_{n+1} - E_n$ that decrease as the quantum number n increases. In such cases, one says that the progression of vibrational levels displays anharmonicity.

Because the Hermite functions H_n are odd or even functions of x (depending on whether n is odd or even), the wave functions $\psi_n(x)$ are odd or even. This splitting of the solutions into two distinct classes is an example of the effect of symmetry; in this case, the symmetry is caused by the symmetry of the harmonic potential with respect to reflection through the origin along the x-axis (i.e., changing x to –x). Throughout this text, many symmetries arise; in each case, symmetry properties of the potential cause the solutions of the Schrödinger equation to be decomposed into various symmetry

groupings. Such symmetry decompositions are of great use because they provide additional quantum numbers (i.e., symmetry labels) by which the wave functions and energies can be labeled.

The basic idea underlying how such symmetries split the solutions of the Schrödinger equation into different classes relates to the fact that a symmetry operator (e.g., the reflection plane in the above example) commutes with the Hamiltonian. That is, the symmetry operator S obeys

$$S H = H S.$$

So S leaves H unchanged as it acts on H (this allows us to pass S through H in the above equation). Any operator that leaves the Hamiltonian (i.e., the energy) unchanged is called a symmetry operator.

If you have never learned about how point group symmetry can be used to help simplify the solution of the Schrödinger equation, this would be a good time to interrupt your reading and go to Chapter 4 and read the material there.

The harmonic oscillator energies and wave functions comprise the simplest reasonable model for vibrational motion. Vibrations of a polyatomic molecule are often characterized in terms of individual bond-stretching and angle-bending motions, each of which is, in turn, approximated harmonically. This results in a total vibrational wave function that is written as a product of functions, one for each of the vibrational coordinates.

Two of the most severe limitations of the harmonic oscillator model, the lack of anharmonicity (i.e., non-uniform energy level spacings) and lack of bond dissociation, result from the quadratic nature of its potential. By introducing model potentials that allow for proper bond dissociation (i.e., that do not increase without bound as $x \rightarrow \infty$), the major shortcomings of the harmonic oscillator picture can be overcome. The so-called Morse potential (see Fig. 2.24)

$$V(r) = D_e (1-\exp(-a(r-r_e)))^2,$$

is often used in this regard. In this form, the potential is zero at $r = r_e$, the equilibrium bond length and is equal to D_e as $r \rightarrow \infty$. Sometimes, the potential is written as

$$V(r) = D_e \ (1\text{-exp}(\text{-a}(r\text{-}r_e)))^2 \text{ -}D_e$$

so it vanishes as $r \rightarrow \infty$ and is equal to $-D_e$ at $r = r_e$. The latter form is reflected in Fig. 2.24.
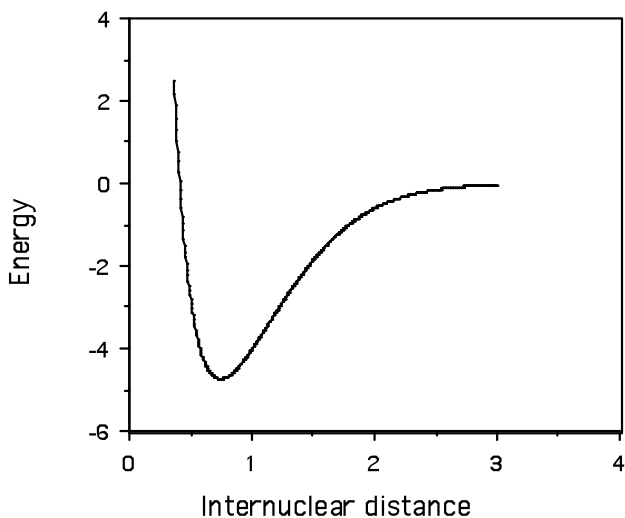

Figure 2.24. Morse potential energy as a function of bond length

In the Morse potential function, D_e is the bond dissociation energy, r_e is the equilibrium bond length, and a is a constant that characterizes the steepness of the potential and thus affects the vibrational frequencies. The advantage of using the Morse potential to improve upon harmonic-oscillator-level predictions is that its energy levels and wave functions are also known exactly. The energies are given in terms of the parameters of the potential as follows:

$$E_n = \hbar(k/\mu)^{1/2} \ \{ \ (n\text{+}1/2) \text{ - } (n\text{+}1/2)^2 \ \hbar(k/\mu)^{1/2}/4D_e \ \},$$

where the force constant is given in terms of the Morse potential's parameters by $k=2D_e$ a^2. The Morse potential supports both bound states (those lying below the dissociation threshold for which vibration is confined by an outer turning point) and continuum states lying above the dissociation threshold (for which there is no outer turning point and thus the no spatial confinement). Its degree of anharmonicity is governed by the ratio of the harmonic energy $\hbar(k/\mu)^{1/2}$ to the dissociation energy D_e.

The energy spacing between vibrational levels n and n+1 are given by

$$E_{n+1} - E_n = \hbar(k/\mu)^{1/2} \{ 1 - (n+1) \ \hbar(k/\mu)^{1/2}/2D_e \}.$$

These spacings decrease until n reaches the value n_{max} at which

$$\{ 1 - (n_{max}+1) \ \hbar(k/\mu)^{1/2}/2D_e \} = 0,$$

after which the series of bound Morse levels ceases to exist (i.e., the Morse potential has only a finite number of bound states) and the Morse energy level expression shown above should no longer be used. It is also useful to note that, if $[2D_e\mu]^{1/2}/[a \ \hbar]$ becomes too small (i.e., < 1.0 in the Morse model), the potential may not be deep enough to support any bound levels. It is true that some attractive potentials do not have a large enough D_e value to have any bound states, and this is important to keep in mind. So, bound states are to be expected when there is a potential well (and thus the possibility of inner- and outer-turning points for the classical motion within this well) but only if this well is deep enough.

The eigenfunctions of the harmonic and Morse potentials display nodal character analogous to what we have seen earlier in the particle-in-boxes model problems. Namely, as the energy of the vibrational state increases, the number of nodes in the vibrational wave function also increases. The state having vibrational quantum number v has v nodes. I hope that by now the student is getting used to seeing the number of nodes increase as the quantum number and hence the energy grows. As the quantum number v

grows, not only does the wave function have more nodes, but its probability distribution becomes more and more like the classical spatial probability, as expected. In particular for large-v, the quantum and classical probabilities are similar and are large near the outer turning point where the classical velocity is low. They also have large amplitudes near the inner turning point, but this amplitude is rather narrow because the Morse potential drops off strongly to the right of this turning point; in contrast, to the left of the outer turning point, the potential decreases more slowly, so the large amplitudes persist over longer ranges near this turning point.

2.10 Chapter Summary

In this Chapter, you should have learned about the following things:

1. Free particle energies and wave functions and their densities of states, as applied to polyenes, electron in surfaces, solids, and nanoscopic materials and as applied to bands of orbitals in solids.

2. The tight-binding or Hückel model for chemical bonding.

3. The hydrogenic radial and angular wave functions. These same angular functions occur whenever one is dealing with a potential that depends only on the radial coordinate, not the angular coordinates.

4. Electron tunneling and quasi-bound resonance states.

5. Angular momentum including coupling two or more angular momenta, and angular momentum as applied to rotations of rigid molecules including rigid rotors, symmetric, spherical, and asymmetric top rotations. Why half-integral angular momenta cannot be thought of as arising from rotational motion of a physical body.

6. Vibrations of diatomic molecules including the harmonic oscillator and Morse oscillator models including harmonic frequencies and anharmonicity.